Energy & Environmental Science

ROYAL SOCIETY OF CHEMISTRY

PAPER

View Article Online
View Journal

Cite this: DOI: 10.1039/d6ee01331g

Environmental and geographic constraints shape global pumped hydroelectric storage for long-duration energy storage

Rongrong Xu, [abc] Zhenzhong Zeng, *[abcjk] Alan D. Ziegler, [d] Lee E. Brown, [e] Joseph Holden, [e] Dominick V. Spracklen, [f] Deliang Chen, [gm] Yuntian Chen,*[bc] Tianyun Dong,[ab] Yaling Zeng,[a] Peirong Lin,[h] Yuan Yang,[il] Ming Pan[il] and Dongxiao Zhang*[bc]

Received 28th February 2026,
Accepted 15th May 2026

DOI: 10.1039/d6ee01331g

rsc.li/ees

Long-duration energy storage is essential for stabilizing electricity systems dominated by wind and solar power, with pumped hydroelectric storage (PHS) as a mature long-duration storage solution. However, the global potential of PHS under realistic hydrological, environmental, and social constraints has not been systematically quantified. Here, we present a global bottom-up assessment integrating hydrology, topography, environment, and transmission accessibility. Screening 2.89 million river and 50 million mountain valleys, we identify 18.82 ± 2.66 PWh of economically and environmentally viable PHS resources that are highly concentrated in mountainous regions. Even under projected cost reductions of competing storage technologies through 2050, PHS remains the most cost-effective option for storage durations exceeding four hours and could deliver over 100 hours of storage for over half of global electricity demand. This study defines a physically constrained benchmark for the role of PHS in future power systems and provides a framework for integrating complementary storage technologies to support resilient, low-carbon electricity systems.

Broader context

Rising electricity demand and rapid expansion of wind and solar power are reshaping energy systems and increasing the need for reliable long-duration storage. Although pumped hydroelectric storage (PHS) is a mature long-duration storage solution, its realistic global role has not been systematically quantified under consistent hydrological, environmental, social, and economic constraints. Here, we present a global bottom-up assessment integrating inundation-based reservoir simulations, environmental and land-use exclusions, and harmonized techno-economic evaluation. By screening 2.89 million river reaches and 50 million mountain valleys, we identified 104 971 PHS candidate projects, with a combined global energy storage capacity of 18.82 ± 2.66 PWh. Our results reveal three insights for energy-system design. First, viable PHS resources are strongly clustered in mountainous regions, creating spatial asymmetry in multi-day storage availability. Second, under projected 2050 cost reductions of competing energy storage technologies, PHS maintains the lowest levelized cost of storage for discharge durations exceeding four hours. Third, transmission distance limits the share of global PHS resources deliverable to demand centers, making moderate grid expansion essential. By releasing this global PHS candidate dataset, our study provides a transparent, consistently constrained resource benchmark to support energy-system modelling, storage technology planning, and transmission expansion analysis.

[a] School of Environmental Science and Engineering, Southern University of Science and Technology, Shenzhen 518055, China. E-mail: zengzz@sustech.edu.cn
[b] Ningbo Institute of Digital Twin, Eastern Institute of Technology, Ningbo 315201, China. E-mail: ychen@eitech.edu.cn, dzhang@eitech.edu.cn
[c] Zhejiang Key Laboratory of Industrial Intelligence and Digital Twin, Eastern Institute of Technology, Ningbo, Zhejiang, China
[d] Andaman Coastal Research Station for Development, Kasetsart University, Ranong, Thailand
[e] School of Geography & Water@Leeds, University of Leeds, Leeds, UK
[f] School of Earth and Environment, University of Leeds, Leeds, UK
[g] Department of Earth System Science, Tsinghua University, Beijing, China
[h] Institute of Remote Sensing and Geographic Information System (IRSGIS), Peking University, Beijing, China
[i] Scripps Institution of Oceanography, University of California San Diego, San Diego, California 92037, USA
[j] State Key Laboratory of Soil Pollution Control and Safety, School of Environmental Science and Engineering, Southern University of Science and Technology, Shenzhen 518055, China
[k] SUSTech Energy Institute for Carbon Neutrality, Southern University of Science and Technology, Shenzhen, 518055, China
[l] Center for Western Weather and Water Extremes, Scripps Institution of Oceanography, University of California, San Diego, La Jolla, CA, USA
[m] Institute for Carbon Neutrality, Tsinghua University, Beijing, China

1. Introduction

Achieving the Paris Agreement's 1.5–2 °C target requires the full implementation of national pledges for sustained emission reductions,[1,2] with the goal of reaching global net zero by 2050. Rising electricity demand, amplified by the rapid expansion of artificial intelligence and digital infrastructure, is creating unprecedented pressure on power systems worldwide.[3] This accelerating demand highlights the urgency of deploying scalable, low-carbon energy sources, placing solar and wind at the center of the global energy transition. However, the rapid integration of renewable energy has introduced new instability into power grids, as supply increasingly fluctuates while demand continues to rise.[4] The coexistence of electricity scarcity and intermittency exposes a fundamental vulnerability in modern energy systems. Stabilizing deeply renewable power systems requires infrastructure that can store electricity from periods of sustained surplus to periods of sustained deficit across multiday timescales.[5]

A diverse range of technologies has emerged to meet the growing need for energy storage in renewable-dominated power systems. Electrochemical batteries, particularly lithium-ion and redox-flow systems, have advanced rapidly and are now widely deployed for short-duration and high-frequency applications, while extending them to multi-day or seasonal balancing is costly and systemically complex.[6,7] Pumped hydroelectric storage (PHS), by contrast, stores energy through gravitational potential between two reservoirs and is characterized by high efficiency, long technical lifetime, and large unit scale, making it well suited for sustained, low-frequency energy shifting over multi-hour to multi-day timescales.[8,9] These attributes have historically positioned PHS as the dominant form of installed grid-scale energy storage worldwide.[10]

While PHS currently accounts for more than 90% of global installed electricity storage capacity,[11] its further expansion is inherently constrained by geography, hydrology, environmental suitability, and social considerations.[12] Meanwhile, rapidly declining electrochemical battery costs and accelerated deployment timelines have intensified competition among storage technologies.[13] Some studies have estimated the potential of closed-loop PHS without accounting for long-term water balance in arid or high-evaporation regions,[14,15] while others have focused on seasonal flow regulation rather than the operational requirements of long-duration energy storage.[16] A systematic understanding of whether the planet contains sufficient economically viable, environmentally acceptable, and hydrologically sustainable PHS resources is missing.

To address this gap, we present a global bottom-up assessment that quantifies the PHS potential under realistic physical, environmental, and economic constraints. We analyzed 2.89 million river[17,18] and 50 million mountain valleys to identify candidate upper and lower reservoir pairs. Each potential site was evaluated based on effective head, topography, water source reliability, and proximity to existing power infrastructure. We constrained siting by avoiding environmentally sensitive regions and limiting population displacement. We performed inundation simulations under varying dam heights and applied a standardized project budgeting framework to estimate the levelized cost of storage (LCOS). Additionally, we examined how future cost reductions in other storage technologies could influence the relative economic competitiveness of PHS. This analysis provides a quantitative basis for understanding how much of the planet's landscape can realistically support large-scale energy storage and for identifying the physical boundaries that constrain high-renewable energy systems.

2. Results and discussion

2.1. Global resources and distribution of PHS

Using inundation simulations and standardized cost modeling under economic, hydrological, environmental, and social constraints, we identified 104 971 PHS candidate projects, with a combined global energy storage capacity of 18.82 ± 2.66 PWh (Fig. 1a, with uncertainty reflecting the vertical elevation error of the MERIT DEM). The identified PHS resources correspond to more than 2300 hours of projected electricity demand in 2050, indicating that despite stringent hydrological and environmental constraints, a substantial amount of PHS resources is available at the global scale. The vast majority of this capacity (18.54 ± 2.59 PWh across 98 503 sites) is provided by open-loop PHS systems, which are hydraulically connected to natural rivers or lakes. By contrast, closed-loop systems, which are hydraulically isolated from natural surface waters and rely primarily on local precipitation to offset evaporation and seepage losses, contribute only 0.27 ± 0.06 PWh across 6468 sites.

The global distribution of viable PHS resources is governed primarily by the interplay between large-scale topography and hydrological reliability (Fig. S1). Asia holds 11.76 ± 1.61 PWh, more than half of the global total, followed by North America (2.97 ± 0.42 PWh) and South America (2.68 ± 0.37 PWh), while Europe, Africa, and Oceania contain substantially smaller resources (Fig. 1b). These continental differences reflect the fact that feasible PHS sites are unevenly distributed across the landscape, forming clusters in regions where steep terrain coincides with stable river systems. The Himalayas and the Tibetan Plateau, the Andes, the Rocky Mountains, and the Alps contain the world's densest storage belts, and their deep valley geometry enables large hydraulic heads at relatively modest inundation volumes, leading to high energy density and low LCOS (Fig. 1c). In contrast, low-relief or arid regions such as parts of western Europe, the Middle East, and northern Africa lack the elevation gradients or hydrological conditions required to support substantial long-duration storage, which leads to intrinsically limited PHS resources.

At the national scale, PHS resources vary widely in both total capacity and storage duration (Table 1 and Table S1). China leads with 5.57 ± 0.74 PWh, accounting for nearly one-third of global PHS resources, followed by Russia (2.16 ± 0.29 PWh) and Canada (1.90 ± 0.24 PWh). Peru, India, and the United States also have substantial resources, each exceeding 0.7 PWh (Table 1 and Table S1). These countries share favorable geographic characteristics, including large elevation gradients, extensive river

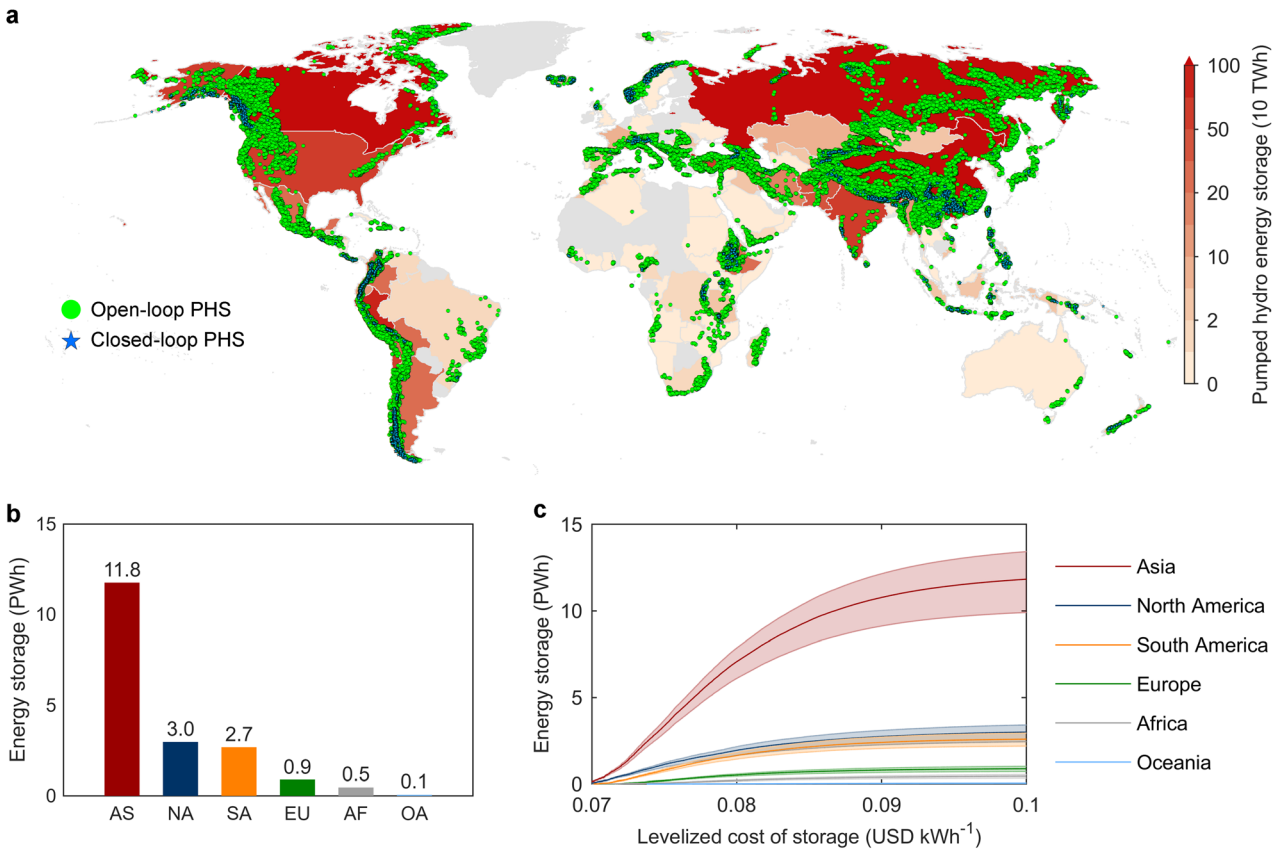

Fig. 1 Spatial distribution of PHS at global and continental scales. (a) Spatial distribution of PHS plants. (b) The PHS potential of each continent. (c) LCOS – storage curves of each continent. AS – Asia, SA – South America, NA – North America, AF – Africa, OA – Oceania, and EU –Europe.

networks, and relatively stable water availability. In contrast, many lowland or arid countries, such as those in the Middle East or northern Africa (Table S1), show much lower PHS potential due to limited precipitation and high evaporation rates.

National differences further shape the effective storage duration that PHS can provide (Table 1 and Table S1). When transmission distance constraints are not considered, the PHS resources of China, Canada, India, and Russia could theoretically provide approximately 2000–7000 hours of storage relative to projected national electricity demand in 2050. However, these resources are often located far from major electricity demand centers, meaning realizing their system-level value depends critically on transmission availability and grid integration. In the United States, PHS resources are also substantial, but higher electricity demand limits the corresponding storage duration to approximately 450 hours. Among other major economies, Japan and Italy benefit from mountainous PHS resources located close to load centers. By contrast, Germany, the United Kingdom, and South Korea can access only a few tens of hours of PHS storage, as limited topographic relief constrains both hydraulic head and reservoir volume (Table S1).

The geographic concentration of viable PHS resources shapes the opportunities and constraints for long-duration storage in renewable-dominated electricity systems. Mountain regions with stable hydrological inputs can support large volumes of low-cost storage, whereas low-relief or water-limited regions have intrinsically constrained PHS potential despite growing demand for long-duration balancing. These spatial patterns highlight that physical availability alone does not determine the contribution of PHS to future energy systems. The economic viability of PHS depends on the interaction between site characteristics, infrastructure requirements, and competing storage technologies.[19] Consequently, assessing the role of PHS in future power systems requires a careful evaluation of both physical constraints and system-level economic trade-offs.

2.2. Cost structure of global PHS resources

To ensure that renewable electricity stabilized by PHS remains low-cost, we adopt LCOS as the primary economic metric.[20,21] LCOS is defined as the discounted cost per unit of discharged electrical energy, accounting for the full capital and operational costs of the PHS system as well as the cost of charging electricity (Table S2). We consider PHS projects with an LCOS below 0.1 USD kWh^{-1} as economically viable, a conservative threshold that keeps storage-stabilized renewable electricity broadly competitive with fossil-based generation.[22–24] Across all viable sites, the median global LCOS is 0.0885 USD kWh^{-1}, with moderate geographic variation. Regions such as the Himalayas, Andes, and Alps exhibit systematically lower LCOS, reflecting the strong hydraulic heads generated by steep terrain and confined valleys. In contrast, the LCOS of PHS projects in lower-relief mountain systems such as the Appalachians can reach 0.1 USD per kWh

Table 1 Pumped hydroelectric storage resource, LCOS, storage duration, and per capita energy storage in the major pumped hydropower countries. The units for total energy storage and per capita pumped storage are terawatt-hours (TWh) and kilowatt-hours (kWh), respectively. Storage duration is the equivalent number of hours that national PHS could meet the projected 2050 electricity demand. LCOS indicates the average LCOS (USD kWh^{-1}) of PHS within each country. Uncertainty ranges are derived from MERIT DEM

Country	Energy storage	LCOS	Storage duration	Per capita energy storage
China	5568 ± 744	0.079	3346	3919
Russia	2162 ± 293	0.080	3969	15 270
Canada	1900 ± 237	0.078	6591	51 488
Peru	969 ± 127	0.079	>8760	30 709
India	722 ± 89	0.080	2129	551
United States	706 ± 113	0.080	445	2157
Chile	665 ± 86	0.079	>8760	36 937
Turkey	507 ± 84	0.080	7867	6246
Kyrgyzstan	475 ± 60	0.080	>8760	81 957
Afghanistan	449 ± 63	0.080	>8760	14 734
Pakistan	391 ± 47	0.080	>8760	1715
Colombia	330 ± 51	0.082	>8760	6806
Ethiopia	292 ± 58	0.081	>8760	2689
Bolivia	284 ± 39	0.079	>8760	24 963
Mexico	281 ± 48	0.081	3400	2208
Nepal	263 ± 33	0.081	>8760	8774
Argentina	262 ± 41	0.080	>8760	5787
Tajikistan	256 ± 32	0.080	>8760	29 377
Italy	192 ± 26	0.080	1399	3103
Norway	188 ± 35	0.079	2422	36 232

(Fig. S2). Larger PHS installations, as illustrated in Fig. S3, benefit from economies of scale, whereby increasing capacity leads to lower LCOS.

We quantified the LCOS components of all candidate PHS sites and evaluated their sensitivity to key cost parameters[22] (Table S3). LCOS is primarily driven by capital-related parameters, with construction costs and interest rates emerging as the most influential variables (Fig. S4). Increasing construction costs by 50% results in a 6.4% increase in average LCOS, and a comparable increase in the interest rate increases LCOS by 7.5%. By contrast, social impacts contribute minimally to LCOS because candidate sites requiring extensive farmland inundation or large-scale population displacement are excluded by siting constraints, with most viable projects associated with fewer than 40 displaced persons per gigawatt of storage capacity (Fig. S5). To further quantify the influence of this social constraint, we conducted a sensitivity analysis by varying the maximum allowable displacement threshold from 0 to 1000 people per reservoir. Global PHS potential stabilizes once the threshold exceeds approximately 200 people, with only modest additional gains (Fig. S6). Most cost-effective PHS sites are located in sparsely populated mountain valleys. Nevertheless, displacement risk remains a site-specific governance constraint, and any development would require local social-impact assessment, resettlement planning, and community consent.

The price of charging electricity introduces an additional but structurally distinct component of PHS cost. In the main assessment, we used a uniform charging electricity price of 0.05 USD per kWh as a harmonized benchmark rather than a site-specific estimate of regional curtailed renewable electricity prices. To assess the sensitivity of this assumption, we decomposed total LCOS into charging-related and infrastructure-related contributions (Fig. S7). The charging-related component increases approximately linearly with electricity price, whereas the infrastructure-related component remains unchanged. Across viable sites, the infrastructure-related contribution of PHS remains approximately 0.024 USD kWh^{-1}, representing the cost of storing and redelivering electricity once infrastructure is deployed. Where wind or solar curtailment creates surplus renewable electricity with low opportunity cost, PHS could approach this infrastructure-related cost floor by using otherwise curtailed generation for pumping.[25] By contrast, where renewable electricity is already well absorbed and pumping depends on higher-priced grid electricity, the cost advantage of PHS would be reduced.

The cost of PHS is shaped by both site-specific infrastructure requirements and the price of charging electricity. Good topography and scale can reduce the infrastructure-related cost floor, while low-cost surplus renewable electricity can further strengthen the economic case for PHS. However, low site-level LCOS alone does not determine system value. The role of PHS in future power systems also depends on how its cost and operating characteristics compare with alternative storage technologies across different discharge durations and cycling frequencies.

2.3. Cost competitiveness of PHS against alternative storage technologies

As global electricity demand grows and renewable penetration increases, the economics of energy storage are becoming central to power-system planning. For PHS, competitiveness depends strongly on operating mode. We evaluated LCOS across discharge durations of 0.25–64 h and annual cycling frequencies of 1–400 cycles per year, showing that LCOS declines with longer discharge duration and higher cycling frequencies (Fig. S8). Under short-duration, low-use conditions, fixed capital costs are spread over limited discharged energy, producing high LCOS, whereas frequently cycled multi-hour systems achieve much lower costs. Against this backdrop, we compared PHS with eight alternative storage technologies, including lithium-ion batteries, flywheels and compressed air storage, by identifying the lowest-LCOS option across the same operating space.[20,21] PHS is most competitive in low-frequency, long-duration applications, where its advantage strengthens with increasing discharge duration, supporting services such as multi-day balancing of renewable generation (Fig. 2). By contrast, lithium-ion batteries and flywheels are more competitive for short-duration, high-frequency (above 400 cycles per year) applications. PHS is less suited to intensive cycling because frequent start–stop operation increases mechanical stress and maintenance costs,[26] whereas electrochemical storage can sustain rapid repeated cycling more efficiently.[27]

As storage technologies continue to evolve,[20,21] the relative competitiveness of different approaches shifts. At the baseline battery cost level (2025; Fig. 2a), PHS retains a cost advantage in low-frequency operational regimes. As the capital costs of lithium-ion batteries and flywheels decline toward 2030 and 2040 (Fig. 2b and c), these technologies become more economically attractive

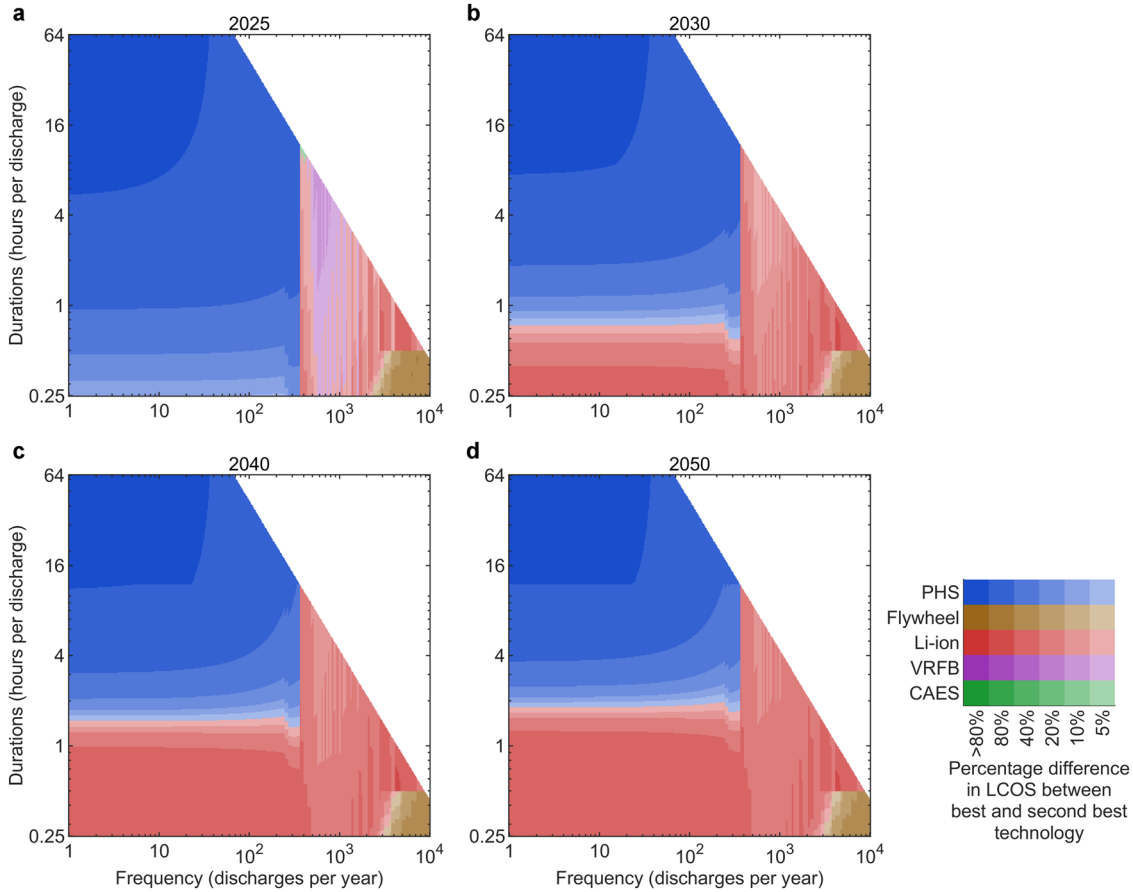

Fig. 2 Cost competitiveness of energy storage technologies across discharge duration and cycling frequency from 2025 to 2050. (a) 2025 cost benchmark. (b) 2030 cost benchmark. (c) 2040 cost benchmark. (d) 2050 cost benchmark. Each panel shows the technology with the lowest LCOS under a given combination of discharge duration and annual cycling frequency. Colors indicate the percentage cost difference between the most competitive technology and the second-best option.

for short-duration and high-frequency (above 400 cycles per year) applications. By 2050, rising global storage demand intensifies cross-technology competition (Fig. 2d). Continued improvements in electrochemical systems erode PHS's advantage in applications with discharge durations of approximately two hours, whereas PHS remains cost-competitive at lower cycling frequencies and discharge durations exceeding three hours, particularly where hydraulic head and project scale reduce LCOS.

Energy storage projects are sensitive to financing conditions because capital costs are recovered over long operating lifetimes. This sensitivity is particularly relevant for PHS, which has high upfront investment but a long technical lifetime (Fig. S4). Using 2050 technology-cost assumptions, we evaluated the lowest-LCOS storage technology at interest rates of 2%, 5%, 8% and 11% (Fig. S9). At a 2% interest rate, PHS becomes cost-competitive at discharge durations of approximately one hour. At 5%, 8% and 11%, the competitiveness boundary remains close to two hours, with only moderate shifts toward longer durations as the interest rate increases. A lower-interest-rate environment would further enhance the advantage of PHS for long-duration storage.

PHS is a key technology for large-scale, long-duration storage, particularly in regions with favorable topography and hydrological conditions. As batteries and flywheels advance, they are likely to capture larger shares of short-duration and high-frequency applications. The effective deployment of these technologies will depend on cost, operational flexibility, and coordinated integration within existing and future power networks.

2.4. Transmission-constrained accessibility of global PHS resources

Although the identified PHS resources correspond to more than 2300 hours of projected global electricity demand in 2050, its effective contribution to power systems is constrained by transmission accessibility.[28] As nearly 87% of suitable PHS sites lie within 100 kilometers of existing high-voltage lines (Fig. S10), much of the world's PHS capacity can be connected to current grid infrastructure with limited network expansion. However, these sites are unevenly distributed across continents, resulting in pronounced mismatches between long-duration storage resources and major demand centers. Transmission infrastructure determines which PHS sites can deliver electricity to load centers and directly shapes the cost of delivered electricity.[29]

To quantify how the service radius of PHS facilities constrains their practical contribution under projected 2050 electricity

demand (Fig. S11), we simulated PHS power delivery within service radii ranging from 100 to 1200 km. In wind- and solar-dominated systems, previous studies show that more than 100 hours of storage may be required to maintain stability during prolonged weather-driven deficits.[30] When PHS is restricted to a 300 km service radius, only 39.7% of global electricity demand gains access to storage exceeding 100 hours, while 31.7% of global electricity demand receives no PHS support (Fig. 3a and Fig. S12a). Expanding the radius to 600 km substantially improves system coverage, enabling 58.4% of global electricity demand to access storage beyond this threshold and reducing unserved regions to 11.5% (Fig. 3b and Fig. S12b). Further expansion to 900 km primarily extends achievable storage duration rather than geographic coverage, increasing the share of demand supported by more than 100 hours of storage from 69% to 77% (Fig. 3c and Fig. S12c). Beyond this distance, marginal system benefits diminish as transmission losses, infrastructure requirements, and operational complexity increase (Fig. 3d and Fig. S12d). The PHS service radius imposes a structural constraint on the usable fraction of global PHS resources, with moderate expansion (approximately 600–900 km) unlocking substantial gains and further extension yielding diminishing returns.

Using projected 2050 cost reductions across a broad range of competing storage technologies as a benchmark,[20,21] we quantified the transmission-adjusted LCOS of PHS under different transmission distances.[31–34] By incorporating distance-dependent line losses and the capital costs of transmission infrastructure, we evaluated the cost competitiveness of PHS relative to alternative storage options. When the transmission distance is set to zero, cross-technology competition in 2050 already erodes the advantage of PHS in applications requiring around two hours of discharge duration (Fig. 2d). When the transmission distance expands from 300 to 1200 km, the boundary of PHS cost competitiveness shifts progressively toward longer discharge durations (Fig. 4a–d). Under these conditions, PHS no longer maintains a cost advantage over short-duration technologies such as lithium-ion batteries for applications requiring roughly two to four hours of discharge, especially when frequent cycling is required. Despite this contraction of its competitive domain at shorter timescales, the advantage of PHS in long-duration, low-frequency applications remains robust. Across all transmission scenarios, PHS continues to provide the lowest LCOS for discharge durations exceeding four hours, with the cost advantage becoming increasingly pronounced for sustained output beyond approximately 16 hours and extending into multi-day timescales (Fig. 4).

Future renewable power systems will rely on coordinated deployment of multiple storage technologies.[35] Rapid cost reductions, modularity, and short construction timelines make

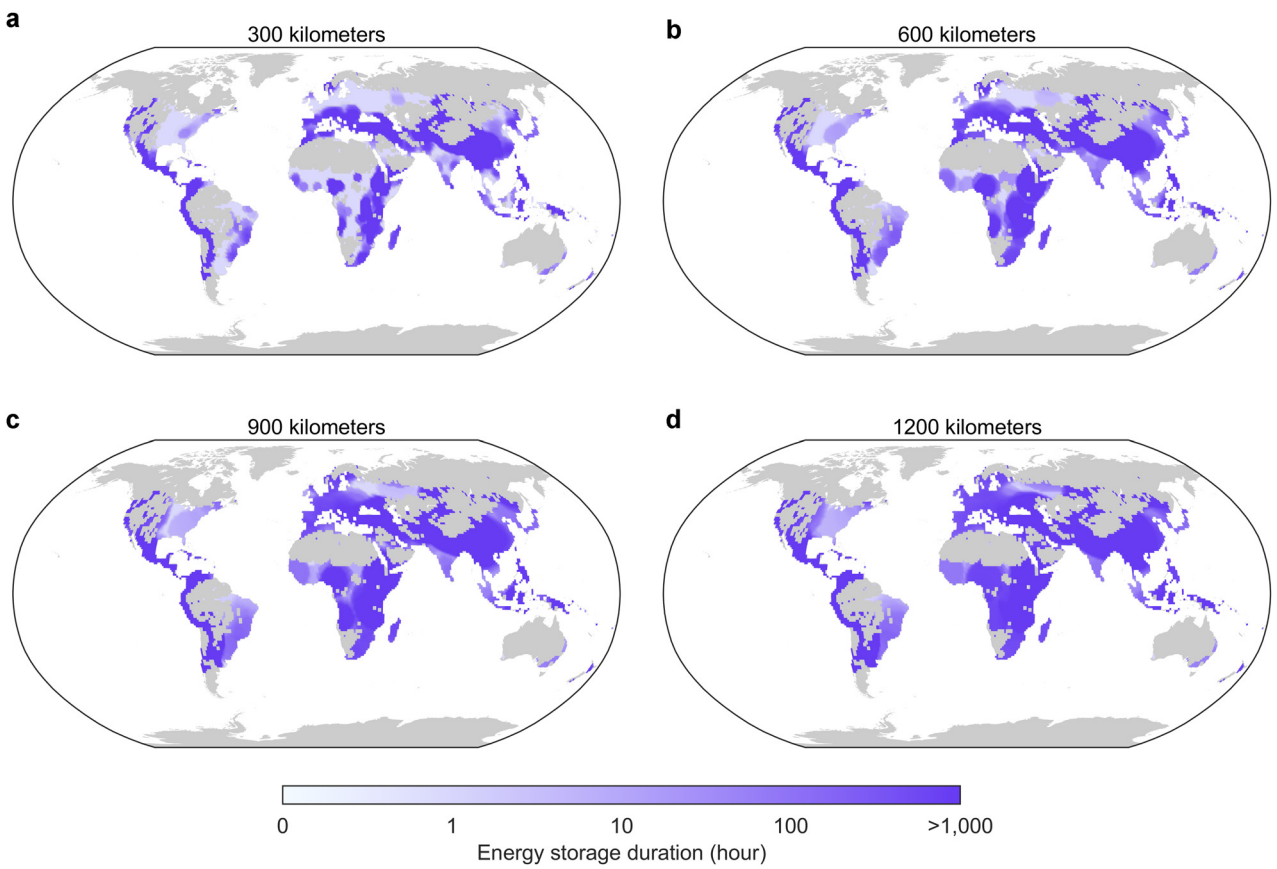

Fig. 3 Spatial distribution of accessible PHS storage duration under different PHS service radii. (a) PHS storage supply within a 300 km service radius. (b) PHS storage supply within a 600 km service radius. (c) PHS storage supply within a 900 km service radius. (d) PHS storage supply within a 1200 km service radius. Gray areas indicate regions with no human activity.

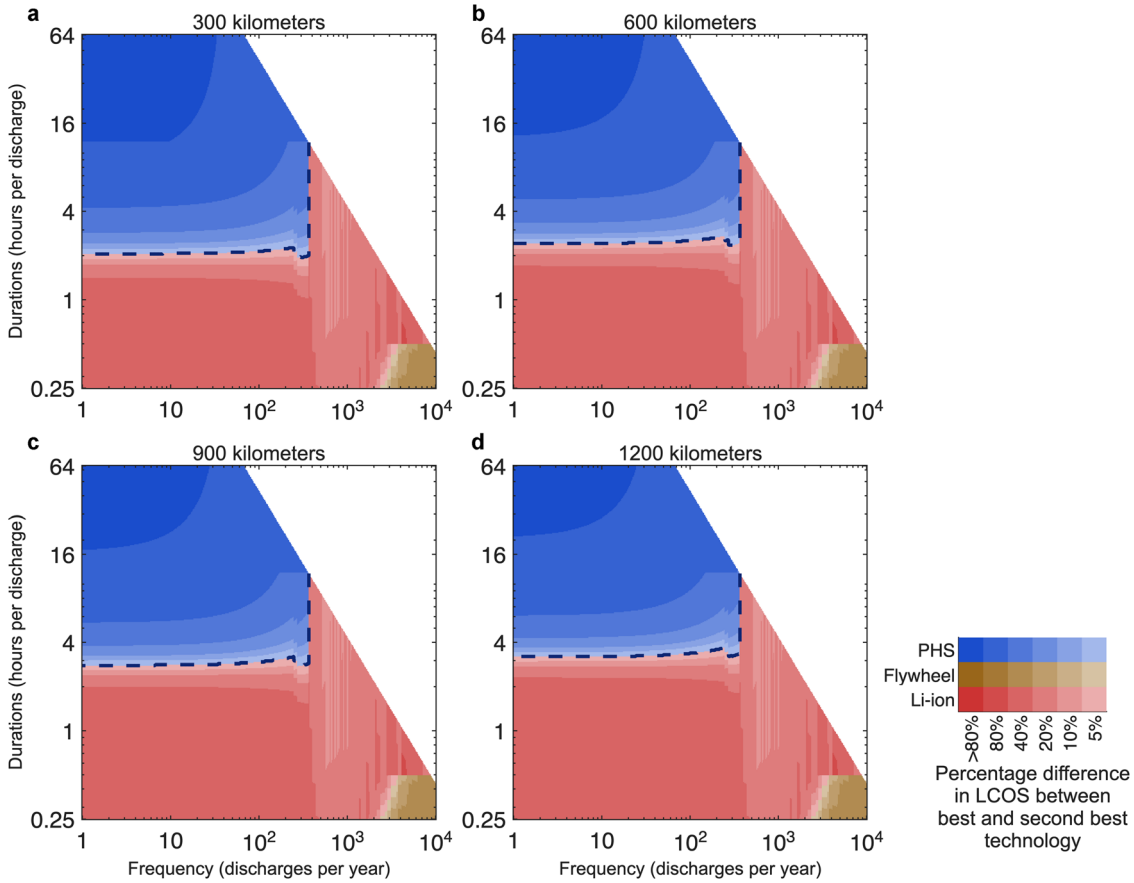

Fig. 4 Cost competitiveness of PHS with transmission-adjusted delivery relative to other energy storage technologies in 2050. (a) 300 km transmission distance. (b) 600 km transmission distance. (c) 900 km transmission distance. (d) 1200 km transmission distance. PHS is evaluated with distance-dependent transmission costs and losses at each prescribed transmission distance. Other storage technologies are assumed to be deployed near electricity demand, such as at the urban fringe or close to load centers, and are assigned a representative delivery distance of 100 km. Colors indicate the percentage cost difference between the most competitive technology and the second-best option. The dashed line marks the boundary at which the cost advantage shifts between PHS and lithium-ion batteries.

electrochemical storage well suited for short-duration and high-frequency (above 400 cycles per year) applications. In contrast, PHS involves large upfront investment, long development timelines, and complex permitting processes, which constrain rapid deployment.[9] PHS plays a complementary role alongside electrochemical batteries, providing large-scale, long-duration balancing where geographic and hydrological conditions permit. Under such coordinated deployment, PHS can continue to deliver substantial system value despite its longer development timelines and higher upfront investment requirements.

2.5. Hydrological, environmental, and governance boundaries of PHS

PHS is inherently a water-based energy storage technology, and its long-term viability depends on local hydrological conditions. Across most viable sites, the water required to offset evaporation and seepage remains modest, typically below 1–2 L kWh^{-1} (Fig. 5a), comparable to or lower than cooling-water use in conventional thermal power generation.[36] Within this range, PHS generally operates within established power-sector water-use norms. Elevated water-use intensities exceeding 2 L kWh^{-1} occur only at a limited number of open-loop sites, mainly in arid or semi-arid mountain regions.

For each open-loop PHS site, we calculated the annual water-use ratio as the net volume of river water needed to compensate for reservoir evaporation and seepage losses, divided by the mean annual river discharge. Open-loop PHS resources are concentrated at low water-use ratios, with 11.01 PWh of open-loop PHS below 20% of mean annual discharge and all open-loop sites below 50% (Fig. S13). The substantial residual river flow remains available to accommodate environmental-flow requirements, although site-specific water scarcity may still constrain PHS development in dry landscapes. Global PHS potential is only moderately sensitive to environmental-flow assumptions, declining from approximately 20.6 PWh to 17.4 PWh when environmental flow is increased to 50% of the multi-year mean annual discharge (Fig. S14).

We further evaluated whether future runoff changes could constrain the long-term operability of open-loop PHS using climate-adjusted discharge projections from seven CMIP6 models[37] under SSP245 and SSP585. This stress assessment shows that 94.8–95.7% of open-loop PHS sites would remain

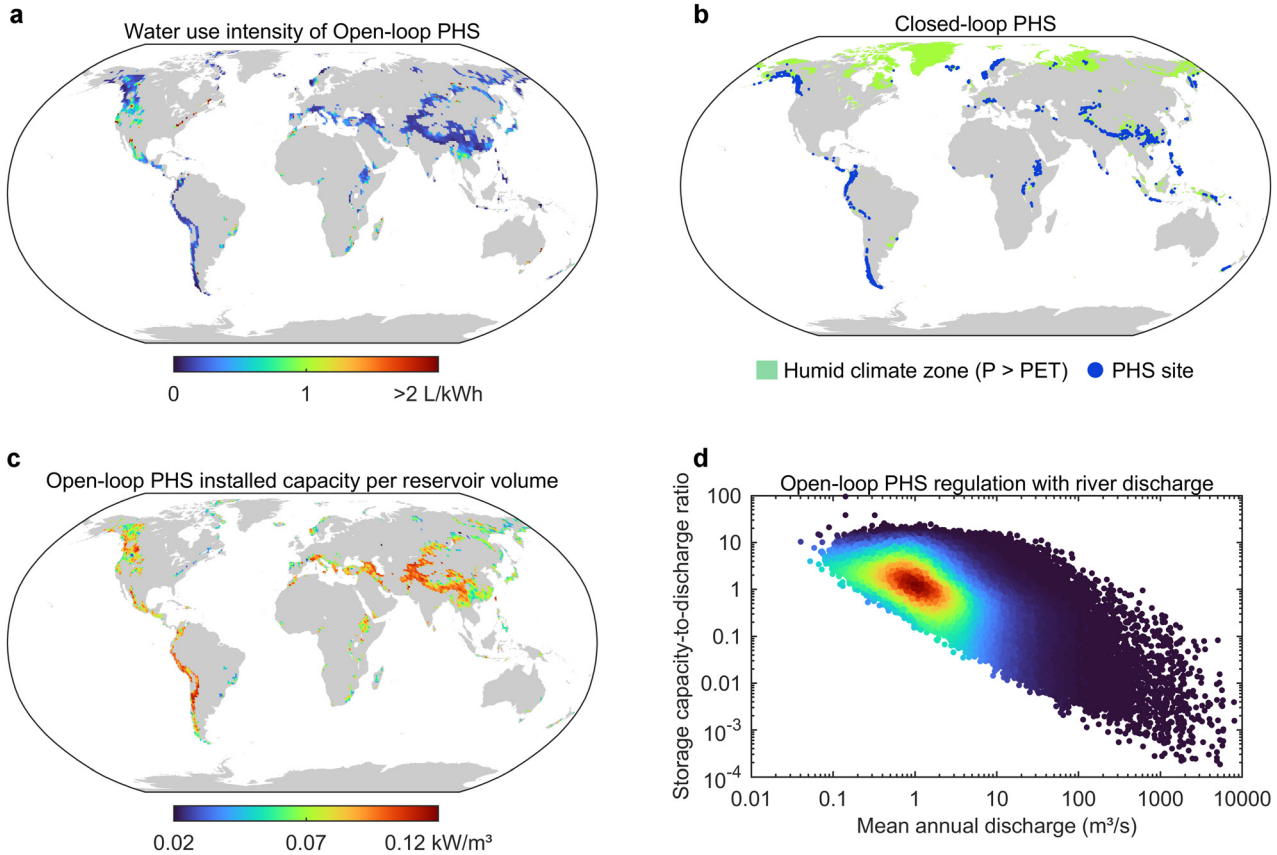

Fig. 5 Hydrological constraints and storage–flow relationships of PHS. (a) Water usage to offset evaporation and seepage per unit electricity generated by open-loop PHS. (b) Global distribution of closed-loop PHS sites constrained to humid climate regions where long-term precipitation exceeds potential evaporation (P > PET). (c) Installed open-loop PHS capacity per unit reservoir volume. (d) Ratio of PHS reservoir storage volume to mean annual river discharge of the host river basin. Gray regions indicate areas without PHS resources.

unconstrained by projected runoff changes. If limited flexibility in environmental-flow allocation is allowed under regulated operation, the unaffected share increases to 99.0–99.6% (Fig. S15). Future water-limited risk is spatially concentrated. The vulnerable sites are mainly located along dry mountain margins in the Mediterranean region and Central and West Asia, where declining runoff could reduce available water for compensating evaporation and seepage losses. By contrast, major PHS-rich regions such as the Himalayas and much of the Andes remain largely unaffected, indicating that future hydroclimatic change is unlikely to substantially reduce the global open-loop PHS resource.

Unlike open-loop systems, closed-loop systems do not rely on continuous river inflow and must sustain long-term operation through local water balance alone.[38] Their hydrological viability requires a positive long-term water balance, with precipitation consistently exceeding potential evaporation and reservoir seepage losses, which confines closed-loop PHS to humid climate regions (Fig. 5b). These hydrological constraints translate directly into systematic differences in scale and cost between open-loop and closed-loop systems. Open-loop systems exhibit larger per-site storage capacities and a broader distribution of low LCOS values, whereas closed-loop systems are characterized by smaller storage volumes and higher LCOS (Fig. S16). Consequently, our estimate of global closed-loop PHS potential is substantially lower than previous assessments, which reported approximately 23 PWh of closed-loop storage across 616 000 sites.[14]

This difference reflects a shift from a topographic opportunity inventory to a hydrologically sustainable and environmentally constrained resource estimate. Stocks *et al.* primarily identified topographically suitable off-river reservoir pairs,[14] whereas our baseline further requires each closed-loop system to maintain a non-negative long-term water balance using local precipitation alone. This distinction is critical because closed-loop PHS, unlike open-loop systems, cannot rely on continuous river inflow to compensate for reservoir water losses. In addition to this water-balance constraint, our assessment explicitly accounts for open-water potential evaporation, engineered seepage losses, environmental exclusions, social constraints, economic screening and spatial consolidation of overlapping candidate sites. The 0.27 PWh estimate represents the hydrologically self-sustaining closed-loop PHS resources under our baseline constraints, not all technically possible closed-loop configurations with external water supply.

To evaluate whether limited supplementary water could expand the feasible closed-loop potential, we simulated annual make-up water allowances equivalent to 0–5% of reservoir volume. Closed-loop PHS potential increases from 0.27 PWh

across 6468 sites under the zero-make-up-water baseline to 1.37 PWh across 18 899 sites under a 5% make-up-water allowance (Fig. S17). This confirms that supplementary water can substantially expand closed-loop feasibility and that the baseline estimate is conservative relative to some engineering practices. However, even under the 5% make-up-water scenario, the estimated potential remains far below the 23 PWh reported by Stocks *et al.*[14] The discrepancy is caused by the combined effects of explicit water-balance constraints, potential evaporation, seepage losses, environmental exclusions, social constraints, economic screening and spatial consolidation.

Reservoir seepage imposes an additional and often decisive constraint on closed-loop PHS. Under stringent seepage control conditions, with daily seepage limited to 0.02‰ through engineered lining and sealing, up to 35 430 closed-loop sites can be identified globally, distributed across most humid regions (Fig. S18 and S19). However, the number of feasible sites declines rapidly as daily seepage rates increase. At a daily seepage rate of 0.4‰, only 2323 sites remain worldwide, confined to a small subset of climatically favorable climatic settings, and their contribution to global PHS energy potential becomes negligible (Fig. S18 and S19). By contrast, open-loop PHS exhibits substantially lower sensitivity to seepage because river inflows compensate for reservoir losses, resulting in comparatively stable site availability and energy potential across seepage scenarios (Fig. S19).

PHS provides not only energy storage but also reservoir capacity that may support ancillary functions such as flood regulation and irrigation.[39,40] The relationship between installed capacity and reservoir volume reflects both the energy density of PHS systems and the scale of water storage inherent to their design (Fig. 5c). Beyond volume alone, the hydrological significance of PHS can be assessed by comparing reservoir storage with mean annual river discharge. This ratio indicates the potential of PHS reservoirs to influence downstream hydrology, including flood attenuation or dry-season flow support (Fig. 5d). Globally, most PHS sites exhibit ratios between 0.5 and 20, suggesting that stored volumes are comparable to or exceed typical annual river flows. Whether this hydrological influence can be realized depends on operational strategies, governance frameworks, and competing water-use priorities.

Hydrological constraints define where PHS can function physically, but they do not alone determine where it can be responsibly developed. Environmental protection and social considerations impose additional landscape-level constraints that further limit deployable PHS capacity. Our framework excludes locations within strict protected areas,[41] UNESCO World Heritage Sites,[42] tropical rainforests,[43] peatlands,[44] and permafrost zones.[45] These exclusions remove sites located in biodiversity hotspots, carbon-dense ecosystems, culturally significant regions, and socially sensitive valleys, restricting PHS deployment to areas with comparatively lower environmental consequences. To quantify the unconstrained physical ceiling, we reassessed the global PHS potential without environmental and environmental-flow exclusions. This assessment yields a theoretical PHS resource of 38.54 ± 5.72 PWh, more than twice the constrained estimate (18.82 ± 2.66 PWh). A substantial portion of physically feasible PHS capacity lies in landscapes where development would conflict with environmental or social safeguards.

Governance frameworks add an additional boundary beyond hydrological and environmental constraints. A subset of PHS resources spatially overlaps with Indigenous territories. Globally, 3048 candidate sites, corresponding to 0.58 ± 0.10 PWh of PHS resources, are located within Indigenous lands[46] (Fig. S20), primarily in western North America, the Andes, and Australia. Consistent with the Free, Prior and Informed Consent (FPIC) principle embedded in the UN Declaration on the Rights of Indigenous Peoples (UNDRIP), whether and how these sites can be developed depends on land-right recognition, water-right governance, benefit-sharing mechanisms, consent processes, and ownership structures.[47] In some regions, Indigenous utility authorities and co-development models are emerging, but regulatory barriers, cultural protections, and the right of communities to reject development may place certain areas entirely off-limits.[48,49] PHS expansion depends on engineering feasibility, environmental safeguards and governance processes that uphold Indigenous sovereignty, procedural justice and community decision-making.

3. Conclusions

Our analysis shows that PHS is a substantial yet inherently bounded component of future low-carbon electricity systems. We identify 18.82 ± 2.66 PWh of PHS capacity that is compatible with hydrological balance and environmental protection, although these resources are concentrated in mountainous regions and unevenly distributed worldwide. Batteries and other fast-responding technologies are essential for short-duration regulation, whereas PHS can deliver cost-effective multi-hour to multi-day balancing. The identified PHS resources provide a physically constrained benchmark for storage planning and a spatial framework for integrating PHS with complementary storage technologies in renewable power systems.

4. Materials and methods

4.1. Overview of the global PHS assessment framework

We developed a global, bottom-up assessment framework to quantify the physically feasible, hydrologically sustainable, and economically deployable potential of PHS under environmental and social constraints. The framework is designed to isolate the contribution of physical geography and water availability to global PHS potential, while minimizing the influence of subjective siting choices or region-specific modeling assumptions.

We distinguish between open-loop and closed-loop configurations.[38] Their hydrological connections determine both environmental-impact pathways and water-sustainability constraints. Open-loop PHS is hydraulically connected to natural rivers or lakes, allowing reservoir water levels to be supported by ongoing inflows, but also creating potential impacts on river-flow regimes, environmental-flow requirements, aquatic habitats and downstream water use. Closed-loop PHS is largely isolated from natural surface waters during normal operation

and has lower direct impacts on river discharge and aquatic connectivity, but its feasibility depends more strongly on local precipitation, evaporation losses and seepage control. Both configurations can cause reservoir inundation, land disturbance, evaporation, seepage losses and landscape modification, and were subject to the same environmental and land-use exclusions. Open-loop systems were further constrained by river-water availability and environmental-flow requirements, whereas closed-loop systems were constrained by hydrological self-sufficiency under precipitation, evaporation and seepage balance.

The assessment proceeds through four sequential stages. First, potential upper-lower reservoir pairs are identified from global river networks and valley landforms. Second, reservoir geometry and storage capacity are quantified through inundation simulations, enabling the estimation of feasible dam heights, reservoir volumes, and associated construction requirements. Third, long-term hydrological feasibility is evaluated by accounting for precipitation, runoff, evaporation, and seepage losses, thereby assessing whether candidate configurations can sustain stable operation under historical hydroclimatic conditions. Finally, candidate systems are integrated into a spatial framework to evaluate their deliverable energy, transmission-constrained accessibility, and LCOS relative to alternative storage technologies.

All analyses are conducted at the global scale using harmonized datasets and a unified cost framework so that differences in estimated PHS potential primarily reflect physical geography, water availability, and explicit environmental and social constraints.

4.2. River discharge, climate, and topographic datasets

PHS reservoirs recycle water during charge–discharge cycles, but their open surfaces expose them to evaporative and seepage losses that accumulate over long time horizons. Global river discharge, climate variables, and topography form the physical basis of the PHS assessment.

To assess whether open-loop PHS systems can be sustained by river inflows under long-term dry conditions, we used the global daily river discharge dataset developed by the Terrestrial Hydrology Research Group at Princeton University, which provides discharge estimates for 2.89 million rivers worldwide over the period 1980–2020 (ref. 17).

To quantify reservoir-scale water inputs and climatic losses for both open-loop and closed-loop PHS systems, we derived precipitation and potential evaporation over the most recent ten years from the ERA5-Land reanalysis dataset at 0.1° spatial resolution.[50] Precipitation represents the dominant atmospheric input to reservoirs, while potential evaporation provides a conservative estimate of evaporative losses from open water surfaces.

To resolve hydraulic head, valley geometry, and inundation extent at the spatial scales relevant to PHS engineering, we employed the Multi-Error-Removed Improved-Terrain digital elevation model (MERIT DEM) at 3 arc-second resolution.[51,52] This high-resolution topographic framework provides the geometric basis for characterizing elevation gradients, delineating potential reservoir basins, and simulating inundation extent across a wide range of dam heights. All subsequent analyses of hydraulic head, reservoir volume, and storage capacity were conducted consistently within this DEM-based spatial framework.

To identify potential reservoir locations that are not sustained by persistent river inflow, we distinguished valley landforms from river networks based on their hydrological function. Although both valleys and river networks represent zones of topographic convergence, they differ fundamentally in upstream contributing area and runoff persistence. Valleys with limited contributing area cannot sustain stable, perennial discharge, whereas river networks with large upstream drainage areas support continuous or intermittent flow. Based on this distinction, we classified convergent features with comparatively small upstream drainage areas as valleys and treated them separately from river networks. Valley landforms were delineated using the MERIT Hydro framework, which derives flow direction and flow accumulation from the MERIT DEM to map surface convergence across near-global coverage (60°S–90°N). Using this approach, we identified approximately 50 million valley features worldwide.

4.3. Engineering and economic feasibility of candidate PHS sites

The engineering and economic evaluation of candidate PHS sites was guided by established PHS siting and design standards. We primarily referenced China's national PHS site selection guidelines,[53] complemented by technical reports from the U.S. Army Corps of Engineers[54] and site selection criteria developed in the Republic of South Africa.[55] These engineering standards provide consistent constraints on reservoir geometry, hydraulic head, dam construction, and system configuration.

To ensure global applicability and spatial consistency, we further incorporated methodological insights from previous studies that employed geographic information system (GIS) techniques to identify suitable PHS locations.[56–60] We used a unified simulation framework for evaluating the engineering feasibility and cost performance of candidate PHS geometries at the global scale. The detailed procedures used to implement this framework are described below.

4.3.1. Identification of candidate PHS. To evaluate the global potential for PHS, we systematically simulated candidate PHS geometries along valley landforms and river networks. Valley and river features were delineated using MERIT Hydro[52] and rasterized at the native 3 arc-second resolution of the MERIT digital elevation model (DEM), ensuring spatial consistency between topography and reservoir simulations. In principle, evaluating every grid cell along these features provides the highest possible geometric resolution for identifying potential reservoir locations.

Potential upper-lower reservoir pairs were constructed for each candidate PHS geometry by searching nearby valley and river features. In total, we evaluated approximately 12.38 million candidate PHS sites worldwide. To avoid PHS configurations with insufficient hydraulic head or excessive frictional head losses along long conveyance systems, we constrained each candidate reservoir pair to elevation differences between 100 and 800 m and limited the distance-to-head ratio to below ten.[56,57] The distance-to-head ratio was defined as the horizontal distance between the paired reservoirs divided by their elevation difference.

At the geometry identification stage, open-loop and closed-loop PHS configurations were treated differently based on their topographic connectivity. For open-loop PHS, at least one reservoir was required to be located on a river network, allowing hydraulic connection to a natural watercourse, while the second reservoir could be situated on either a river network or a valley. In contrast, closed-loop PHS geometries were restricted to configurations in which both reservoirs were located within valley landforms, with no direct hydraulic connection to river networks.

4.3.2. Pumped hydroelectric storage calculations. For each candidate PHS geometry, the theoretical storage capacity was calculated based on the effective hydraulic head between the paired reservoirs and the usable storage volume. The effective hydraulic head was defined as the elevation difference between the upper and lower reservoirs, derived from the MERIT DEM and adjusted to reflect the mean operating water levels of each reservoir.

The energy storage capacity of PHS E (kWh) is calculated using:

$$E = \rho VgH/3\,600\,000 \quad (1)$$

where H is the hydraulic head (m) of the PHS plant, V is the reservoir's volume (m^3), g is the gravitational acceleration constant, and ρ represents the density of water. For freshwater, ρ is taken as 1000 kg m^{-3}, and 3 600 000 is the conversion factor from joules to kilowatt-hours.

4.3.2.1. Reservoir volume estimation. Reservoir volume was obtained from the inundation simulations described in the following section, allowing storage capacity to vary continuously with dam height and reservoir geometry. The volume of reservoir V (m^3) is calculated using:

$$V = \min(V_{up}, V_{down}) \quad (2)$$

where V_{up} is the volume of the upper reservoir and V_{down} is the volume of the lower reservoir.

The maximum volume of an individual reservoir was calculated by integrating the inundated area over elevation:

$$V_{reservoir} = \int \left(\mathrm{DEM}(X, Y) + \text{H-DEM}(i) - \delta_{ip}\right) \mathrm{d}S_i \quad (3)$$

where DEM(X,Y) is the elevation at the dam location, H is the dam height, DEM(i) is the elevation of the inundation raster and dS_i is the area of the inundation raster. δ_{ip} represents the maximum ice thickness for the PHS during its coldest month.

In cold and high-latitude regions, seasonal freezing of PHS reservoirs reduces the effective water volume available for energy storage. To account for this effect, the ice-covered portion of the reservoir during the coldest month is excluded from the storage volume calculation. The effective frozen volume is estimated using the maximum seasonal ice thickness, δ_{ip}, which represents the upper bound of ice accumulation under cold-season conditions. This treatment follows established reservoir design methodologies that relate maximum ice thickness to local climatic and operational factors, including air temperature, water temperature, reservoir operating frequency, and daily water-level fluctuations. The method for calculating the maximum ice thickness δ_{ip} can be found in ref. 61.

Uncertainty in topographic representation is addressed by incorporating the vertical error of the MERIT DEM. Given a reported mean elevation error of ±1.09 m and a 90th percentile error of 12 m, we adopt a conservative ±12 m adjustment in DEM(X,Y) to avoid systematic overestimation of storage capacity at the global scale.[51,52]

4.3.2.2. Hydraulic head. Water conveyed through headrace tunnels and penstocks experiences frictional losses. The effective hydraulic head was calculated using:

$$H = H_{geo} - h_f \quad (4)$$

The hydraulic head available for energy conversion in a PHS system is determined by the elevation difference between the upper and lower reservoirs after accounting for hydraulic losses along the conveyance system. The geometric hydraulic head H_{geo} was calculated as the elevation difference between the upper and lower reservoirs:

$$H_{geo} = H_{up} + H_{updam}/2 - H_{down} - H_{downdam}/2 \quad (5)$$

where H_{up} is the elevation of the upper reservoir, H_{down} is the elevation of the lower reservoir, H_{updam} is the height of the upper reservoir's dam, and $H_{downdam}$ is the height of the lower reservoir's dam.

Hydraulic losses h_f in the water conveyance system were estimated using the Darcy–Weisbach formulation. The head loss h_f along the conduit connecting the two reservoirs is given by:

$$h_f = \lambda \frac{l}{d} \frac{Q_D^2}{2g} \quad (6)$$

where λ is the Darcy friction factor, d is the pipe diameter (meter), g is the gravitational acceleration, and Q_D ($m^3\ s^{-1}$) is the design discharge of the PHS system. l is the distance between the upper and lower reservoirs. The design discharge Q_D was derived from the effective reservoir storage volume assuming a complete discharge over a characteristic operation duration:

$$Q_D = \frac{V}{T \times 3600} \quad (7)$$

where V is the effective reservoir volume defined in eqn (2), and T is the discharge duration (hours). To enable economic comparison with other energy storage technologies, T was fixed to approximately 8 hours as a standardized benchmark commonly used in comparative LCOS studies.[20,21] Additional sensitivity analyses spanning 0.25–64 h discharge durations were conducted to evaluate robustness (Fig. S8).

To balance frictional head losses and conveyance construction costs, we optimized the water-conveyance design for each candidate PHS site using one to four parallel tunnels or penstocks. The diameter of each conduit was allowed to vary from 1 meter to 16.7 meter, where the upper bound corresponds to the largest documented hydropower water-conveyance tunnel currently in operation, such as that of the Yinliangbao Hydropower Station.

The conduit number and diameter combination that minimized the site-specific LCOS was selected for each candidate site.

4.3.3. Reservoir inundation simulations. The storage capacity of PHS systems depends on reservoir geometry, which is primarily controlled by dam height and local topography. To quantify reservoir extent and storage volume consistently across all candidate sites, we performed reservoir inundation simulations using high-resolution digital elevation data.

Inundation simulations were conducted based on the MERIT digital elevation model (DEM) at 3 arc-second resolutions. For each candidate reservoir location, a virtual dam was placed at the outlet point of a valley or river reach. Dam heights ranging from 10 to 300 m were evaluated to capture the full range of plausible engineering configurations. For a given dam height, the corresponding reservoir water surface elevation was defined as the local terrain elevation at the dam site plus the dam height.

Reservoir inundation was simulated using a connectivity-constrained flooding algorithm.[22] Starting from an initial upstream seed point located within the same valley or river system, all DEM grid cells with elevations below the water surface were identified as potentially inundated. To ensure physical plausibility, newly inundated cells were required to be directly connected to the existing flooded region. This connectivity constraint prevents unrealistic inundation across adjacent but hydrologically disconnected basins and ensures that reservoir extents reflect feasible water impoundment. The inundation process continued iteratively until no additional connected grid cells satisfied the elevation criterion. For each dam height scenario, the inundated area was calculated as the sum of all flooded grid-cell areas, and the reservoir storage volume was obtained by integrating the elevation difference between the water surface and the underlying terrain across all inundated cells. This procedure yields a continuous relationship between dam height, inundation area, and storage volume for each candidate reservoir. Inundation simulations were performed independently for the upper and lower reservoirs of each candidate PHS site. The resulting reservoir volumes provide the geometric basis for subsequent calculations of energy storage capacity and economic performance.

The broad dam-height range was used to allow candidate reservoirs to reach economically efficient storage scales under local topographic constraints. Larger PHS reservoirs generally benefit from scale-related cost reductions. Consequently, a substantial share of PHS potential is associated with dams above 100 meters, accounting for 68% of candidate sites and 92% of storage energy. In addition, 7% of candidate sites and 22% of storage energy are associated with the 300-meter upper-bound scenario (Fig. S21). This upper bound represents a practical engineering limit in global screening rather than a prescriptive design choice. In site-specific planning, maximum dam height would depend on local engineering feasibility, regulatory requirements, landscape impacts, and social acceptance.

4.3.4. Levelized cost of storage (LCOS) of the PHS. The economic performance of each candidate PHS site was evaluated using LCOS, defined as the average cost per unit of electricity discharged over the operational lifetime of the storage system. LCOS integrates capital investment, operation and maintenance expenditures, charging costs, system lifetime, and energy throughput, enabling consistent comparison across storage projects of different scales and configurations.[20,21] LCOS was calculated using a discounted lifetime formulation:

$$\mathrm{LCOS} = \frac{C_{\mathrm{I}} + \sum_{t=0}^{n}\left(M_t(1+r)^{-t}\right) + \sum_{t=0}^{n}\left(C_{\mathrm{ch}}(1+r)^{-t}\right)}{\sum_{t=0}^{n}\left(E_{\mathrm{E}}(1+r)^{-t}\right)} \quad (8)$$

where C_{I} is the capital investment of the PHS system, M_t is the annual operation and maintenance expenditure, C_{ch} is the annual charging cost, and E_{E} is the annual discharged electricity. r is the interest rate (0.08) and n represents the operational lifetime of the PHS system (55 years). To ensure consistency with LCOS comparisons across other energy storage technologies, both the interest rate and operational lifetime were adopted from ref. 20.

Annual discharged electricity was estimated using:

$$E_{\mathrm{E}} = E \times N \times \eta \quad (9)$$

where E is the energy storage capacity of the PHS system and η is the round-trip efficiency, assumed to be 0.78 (ref. 20). Following typical PHS operational practice reported in the literature, N is fixed to represent typical daily operation, yielding a standardized estimate of annual discharged electricity.

The annual charging cost C_{ch} is calculated using:

$$C_{\mathrm{ch}} = p \times E_{\mathrm{E}}/\eta \quad (10)$$

where η is the efficiency of PHS plants, assumed to be 0.78 (20). E_{E} is the annual discharged electricity. To ensure global consistency and comparability across storage technologies, a constant charging electricity price of 0.05 USD per kWh was applied to all candidate sites.

Capital expenditures for each candidate PHS project were decomposed into power-related and storage-related components to reflect the physical structure of PHS systems.[22–24] Power-related costs include turbine units, electro-mechanical equipment, powerhouse construction, tunnels, penstocks, fish passage facilities, and grid interconnection infrastructure. Storage-related costs include dam construction, land acquisition within the inundation area, population displacement compensation, and seismic hazard mitigation. Each cost component was calculated using empirically derived or engineering-based formulations that link cost to site-specific physical parameters, such as hydraulic head, design discharge, dam height and length, reservoir inundation area, tunnel length, and distance to the nearest transmission line.

All cost formulations, parameter definitions, units, and reference sources are summarized in Table S2. The equations listed in Table S2 were compiled from established PHS cost studies, national engineering standards, and technical reports, and were applied consistently across all candidate sites to ensure comparability of LCOS estimates.[20–24] Composite cost terms, including seismic hazard allowances, owner's costs, and annual operation and maintenance expenditures, were calculated as fixed proportions of total capital investment following standard practice in global hydropower assessments. To maintain a unified and

consistent benchmark for global PHS assessments, owners' costs and annual operation and maintenance expenditures, which are largely independent of site-specific topographic and hydrological conditions, were represented using uniform parameters across all sites. Final LCOS values were obtained by dividing the discounted lifetime project costs by the discounted lifetime discharged electricity. Uncertainties in construction costs and other parameter sensitivities were evaluated through additional sensitivity analyses, with results summarized in Table S3 and Fig. S4.

4.4. Environmental and hydrological constraints

4.4.1. Environmental and land-use constraints. To limit ecological disturbance and social impacts, we defined a set of environmental and land-use constraints that restrict where PHS reservoirs can be developed. These constraints specify landscapes where large-scale reservoir construction would conflict with conservation priorities, sensitive ecosystems, or unacceptable social disruption.

Hard exclusion criteria were first applied to protected and environmentally sensitive areas. These include all categories I, II, III, IV, V, VI of the World Database on Protected Areas,[41] encompassing strict nature reserves, wilderness areas, national parks, natural monuments, habitat and species management areas, protected landscapes, and areas designated for sustainable resource use. UNESCO World Heritage Sites[42] were also excluded. Additional exclusions were applied to high-value tropical rainforests[43] and peatlands[44] critical for biodiversity conservation and long-term carbon storage, and permafrost regions[45] characterized by geotechnical instability. Candidate sites were further excluded where reservoir inundation would result in the displacement of more than 1000 people, reflecting a conservative threshold for social acceptability.[62]

Environmental and social constraints were evaluated in conjunction with the reservoir inundation simulations described in Section 4.3.3. For each candidate site, inundation extents were simulated across a range of dam heights, and feasibility was assessed by examining whether the resulting flooded area intersected any restricted land-use category or exceeded the population displacement threshold. Sites located entirely within exclusion zones were removed from consideration, while sites whose inundation footprints encroached upon restricted areas were deemed infeasible at the corresponding dam heights.

Beyond these hard exclusions, geological and seismic conditions were incorporated as cost-related constraints. Regions underlain by unconsolidated soils were identified using the Harmonized World Soil Database[63] and assigned higher construction costs due to increased foundation and stabilization requirements. Seismic hazard was evaluated using the global seismic hazard map,[64] with areas exhibiting peak ground acceleration exceeding 0.7 m s^{-2} requiring additional seismic reinforcement measures. These factors were reflected as cost penalties in the economic assessment.

For candidate reservoirs that satisfied environmental and social constraints, land-use composition within the inundation area was quantified to estimate compensation costs associated with dam construction. Forests, cropland, grasslands, and displaced population within the flooded footprint were identified for each feasible dam height. Compensation costs for cropland and grasslands were assigned using region-specific land value data, including 2024 state-level values for the United States,[65] provincial values for Canada,[66] and national agricultural land prices for Australia and major EU countries.[67] For regions lacking publicly available land price data, global average cropland and grassland values reported by the USDA were applied. Population displacement costs were estimated based on per-capita GDP.[68] All cost formulations and parameter definitions are summarized in Table S2.

4.4.2. Hydrological sustainability constraints. A sustainable PHS system requires a reliable long-term water balance to compensate for reservoir water losses through evaporation and seepage. To evaluate hydrological sustainability consistently at the global scale, we quantified both loss and input terms under conservative assumptions designed to ensure stable operation during prolonged dry conditions.

Open-loop and closed-loop PHS systems differ fundamentally in their water-supply mechanisms. Open-loop systems are hydraulically connected to natural river networks and can compensate reservoir water losses through both local precipitation and regulated river discharge. Closed-loop systems are hydraulically isolated from natural surface waters and, in the baseline assessment, rely exclusively on direct precipitation over the reservoir surface to offset evaporation and seepage losses. Closed-loop configurations requiring artificial water supplementation are excluded from the baseline estimate. For closed-loop PHS, we further considered annual make-up water allowances equivalent to 0–5% of reservoir storage volume to evaluate the influence of external water availability. For each candidate closed-loop site, the annual water balance was recalculated as precipitation plus the prescribed make-up water allowance minus potential evaporation and seepage losses. Sites were retained only when this adjusted water balance remained non-negative and all engineering, environmental, social and economic constraints were satisfied. The zero-make-up-water case corresponds to the baseline closed-loop estimate reported in the main assessment.

Reservoir water losses were represented by two dominant processes: seepage and evaporation. Seepage control is a standard engineering requirement for PHS reservoirs and is implemented through lining and barrier systems to reduce dependence on local geological conditions. Allowable seepage is governed by design standards. In China, where PHS projects span a wide range of geological settings, reservoir design standards require that post-treatment daily seepage does not exceed 0.2‰ of total storage capacity.[69,70] Accordingly, we adopted 0.2‰ of total storage capacity as the baseline seepage rate in our global simulations. This assumption provides a standardized engineering benchmark. To assess the robustness of this assumption, we conducted a sensitivity analysis across a plausible range of daily seepage rates from 0.02‰ to 0.4‰, spanning scenarios from high-standard seepage control to the upper limit of acceptable reservoir leakage. This sensitivity analysis quantifies the influence of seepage uncertainty on PHS feasibility and global storage potential.

Evaporative losses were estimated using potential evaporation derived from the ERA5 hourly single-level dataset.[45]

Potential evaporation represents the maximum evaporative demand imposed by atmospheric conditions on an open water surface and provides a conservative estimate that avoids underestimating water losses in energy-limited or arid regions.

Water input to PHS reservoirs was supplied by local precipitation and, for open-loop systems, by regulated river discharge. Precipitation was derived from ERA5 hourly total precipitation data, while river inflows were obtained from the global discharge dataset described in Section 4.2.

To impose a conservative constraint on long-term water availability, all hydrological calculations used the driest year within the 41-year record from 1980 to 2020 for each river basin.[17] Allowable river withdrawal was constrained by environmental-flow requirements estimated using both the Tennant and Tessmann methods[71–73] (Table S4). For each site, the maximum allowable withdrawal was calculated separately using the Tennant and Tessmann methods, and the mean of the two estimates was used as the available river withdrawal required to maintain minimum environmental flows. An open-loop PHS site was classified as hydrologically viable only when annual precipitation plus allowable river withdrawal exceeded annual evaporation and seepage losses. To evaluate sensitivity to environmental-flow assumptions, we varied required environmental flow from 0% to 50% of multi-year mean annual flow. At each level, available withdrawal was recalculated and sites were reassessed under the same engineering, hydrological, environmental, social and economic constraints, yielding changes in storage potential and station count.

To assess whether baseline hydrological feasibility remains robust under future hydroclimatic change, we conducted a CMIP6-based future water-stress analysis for open-loop PHS sites. The analysis used monthly runoff projections from seven CMIP6 models,[37] including BCC-CSM2-MR, CESM2, CNRM-CM6-1, HadGEM3-GC31-LL, MIROC6, MPI-ESM1-2-LR and NorESM2-LM, under SSP245 and SSP585. Historical simulations for 1985–2014 and future projections for 2016–2050 were used. Because CMIP6 runoff fields are too coarse to directly represent site-scale river discharge, we applied a relative-change scaling approach. For each model, monthly runoff was aggregated to annual runoff and normalized by the model-specific historical mean annual runoff, yielding an annual runoff-change factor for 2016–2050. This factor was then used to scale the baseline discharge record from the main assessment and generate a climate-adjusted annual discharge series for each model. The seven model-specific series were averaged to obtain an ensemble-mean future discharge series for each scenario. For each open-loop PHS site, annual water requirement was compared with both climate-adjusted total river flow and climate-adjusted available flow after maintaining environmental-flow requirements. The driest year during 2016–2050 was used as the future water-stress condition, and sites whose water requirements exceeded future water availability were classified as future water-limited.

4.5. Site consolidation and global optimization of PHS deployment

Through the procedures described above, we obtained site-specific estimates of LCOS for all candidate PHS after accounting for engineering feasibility, hydrological sustainability, environmental exclusions, and land-use compensation. Owing to the dense sampling of valleys and river networks, this process yielded a large number of technically and economically viable candidates, many of which represent spatially redundant alternatives.

To derive a realizable and non-redundant deployment portfolio, we applied a cost-prioritized site consolidation procedure. Candidate PHS sites were ranked globally by LCOS, from lowest to highest. Starting with an empty global map, sites were sequentially placed beginning with the lowest-cost PHS configuration. A site was retained only if its spatial footprint did not overlap with that of any previously selected site. This iterative placement continued until the LCOS of candidate sites exceeded 0.1 USD kWh^{-1}. Fig. S22 illustrates a portion of the selected PHS plant locations.

We used LCOS as the primary ranking criterion because the identified global PHS resources is already large relative to present electricity-system storage requirements, making cost competitiveness more relevant than maximizing physical storage alone. To quantify the sensitivity of the results to alternative optimization priorities, we repeated the consolidation by prioritizing maximum energy storage potential among sites below 0.1 USD per kWh. This alternative rule produced a similar supply curve to the LCOS-prioritized result, with only modest differences in cumulative storage potential (Fig. S23). We further evaluated algorithmic robustness using an integer-programming validation in Madagascar, where the candidate-site scale was computationally tractable. The integer-programming formulation prioritized low-LCOS sites under spatial non-overlap constraints, and the resulting site portfolio was consistent with the LCOS-prioritized greedy selection. These analyses indicate that the greedy consolidation approach provides a robust and computationally efficient approximation for estimating non-overlapping, cost-competitive PHS potential at the global scale.

The geographic information and key attributes of the 104 971 candidate PHS projects identified in this study are available at https://doi.org/10.6084/m9.figshare.32288043.

4.6. LCOS assessment for alternative energy storage technologies

To enable an unbiased economic comparison across fundamentally different energy storage technologies, we applied a unified discounted lifetime LCOS framework to all systems. For each technology, LCOS was calculated as the discounted sum of capital investment, annual operation and maintenance expenditure, and charging cost, divided by the discounted electricity discharged over the system lifetime (eqn (8)). Using an identical formulation across technologies avoids technology-specific modeling bias and ensures that observed LCOS differences arise from intrinsic technical and cost characteristics.[20,21]

To maintain methodological consistency with established cross-technology assessments, the comparative analysis followed the parameterization reported in ref. 20. Eight representative storage technologies were evaluated, including compressed-air energy storage, flywheels, lead-acid batteries, lithium-ion batteries, sodium-sulfur batteries, redox-flow batteries, hydrogen storage,

and supercapacitors. Technology-specific parameters, including investment cost per unit power (USD per kW), investment cost per unit energy (USD per kWh), annual operation and maintenance cost, round-trip efficiency, and calendar lifetime, were adopted directly from Tables S3 and S4 in ref. 20. For battery-based systems, degradation effects were incorporated following the cycle-life data reported in Table S5 of ref. 20. Projected technology improvement trajectories for 2025, 2030, 2040, and 2050 were taken from Table S7 of ref. 20.

For PHS, we calculated LCOS for 104 971 economically viable sites retained after global screening and spatial optimization, and used their mean LCOS to represent PHS performance in the cross-technology comparison. Capital investment and operation and maintenance costs for PHS were determined endogenously based on reservoir geometry, hydraulic head, inundation extent, and infrastructure accessibility, while all remaining technical and financial parameters, including round-trip efficiency, calendar lifetime, and interest rate, were kept consistent with ref. 20.

To ensure comparability under identical operating conditions, all storage technologies were evaluated using a uniform charging electricity tariff of 0.05 USD kWh^{-1}. LCOS was computed within a two-dimensional utilization space defined by discharge duration ranging from 0.25 to 64 hours and annual cycling frequency from 1 to 10 000 cycles per year. Discharge durations substantially longer than multi-day operation were excluded from the comparative analysis, as extended water residence times in PHS reservoirs amplify cumulative evaporation and seepage losses and may introduce additional water-quality management challenges. Under this harmonized framework, variations in LCOS reflect fundamental differences in efficiency, degradation behavior, capital cost structure, and technical lifetime, enabling a consistent comparison of PHS with alternative energy storage technologies.

4.7. Storage time mapping and transmission-adjusted LCOS of PHS

4.7.1. Calculation of spatial storage time under PHS service radius constraints. We quantified the spatial distribution of PHS storage time by allocating accessible storage energy to electricity demand under PHS service radius constraints. Transmission radii ranging from 100 to 1200 kilometers were considered to represent the operational scale of power delivery, where a radius of 0 km corresponds to local utilization without interregional transmission, and larger radii progressively incorporate long-distance power transfer.

Electricity demand was characterized using a global 1 km × 1 km gridded electricity consumption dataset calibrated by harmonizing DMSP/OLS and NPP/VIIRS nighttime light observations. The 2019 electricity consumption surface was used as the spatial baseline.[74] To represent future system conditions, total electricity demand was uniformly scaled so that its global sum matches projected electricity consumption in 2050, while the spatial distribution of demand was preserved.[28]

For each PHS facility, we identified all electricity demand grid cells located within the specified service radius and calculated the total demand within this area. The storage energy capacity of each PHS facility was then allocated to the surrounding grid cells in proportion to their electricity demand. This demand-weighted allocation procedure was applied independently to all PHS facilities, and storage contributions from multiple facilities were summed for each grid cell. Spatial storage time was calculated for each grid cell as the ratio of allocated PHS storage energy to its annual electricity consumption, expressed as equivalent hours by normalizing with 8760 hours per year.

4.7.2. Calculation of transmission-adjusted LCOS under varying transmission distances. To quantify the economic cost of electricity delivered from PHS to demand centers under transmission distance constraints, we defined a transmission-adjusted LCOS. Transmission-adjusted LCOS represents the discounted lifetime cost per unit of electricity received at the load. To account for the distinct cost and loss characteristics of alternating-current and high-voltage direct-current transmission, the assessment includes both high-voltage direct current (HVDC) and high-voltage alternating current (HVAC) transmission options. For each prescribed transmission distance, the transmission-adjusted LCOS was evaluated under both technologies and retained the lower-cost option.

For a given transmission distance d and transmission technology k, transmission-adjusted LCOS of PHS was calculated as:

$$\mathrm{LCOS}_{\mathrm{del}}(d) = \frac{C_{\mathrm{I}} + C_{\mathrm{tr},k}(d) + \sum_{t=0}^{n}\left(M_t(1+r)^{-t}\right) + \sum_{t=0}^{n}\left(C_{\mathrm{ch}}(1+r)^{-t}\right)}{\sum_{t=0}^{n}\left(E_{\mathrm{E}}(1+r)^{-t}\right)\eta_k(d)} \tag{11}$$

where d is the transmission distance between the PHS facility and the demand center. k denotes either HVAC or HVDC. $C_{\mathrm{tr},k}(d)$ is the technology-specific transmission capital cost at distance d. $\eta_k(d)$ is the delivered-energy efficiency of the corresponding transmission technology over distance d. Definitions of the remaining parameters are consistent with those used in eqn (8).

For HVAC transmission, the transmission capital cost was represented as a distance-proportional line cost:

$$C_{\mathrm{tr,AC}}(d) = p_{\mathrm{AC}}\mathrm{d}N \tag{12}$$

where p_{AC} is the unit construction cost of HVAC transmission per kilometer and N is the ratio between the installed capacity of the PHS facility and the reference transmission capacity. Following the original transmission-cost setting, p_{AC} was set to 1.6 million USD km^{-1}, based on U.S. National Grid data for a medium-capacity two-circuit configuration, with each circuit rated at 3190 MW, corresponding to a total reference transmission capacity of 6.38 GW.[32] HVAC transmission losses were represented as:

$$\eta_{\mathrm{AC}}(d) = 1 - \lambda_{\mathrm{AC}}d \tag{13}$$

where λ_{AC} was set to 0.00007 km^{-1}, corresponding to approximately 7% loss per 1000 km.

For HVDC transmission, we included both distance-proportional line costs and terminal converter costs:

$$C_{\mathrm{tr,DC}}(d) = (p_{\mathrm{DC}}d + 2C_{\mathrm{conv}})N \tag{14}$$

where p_{DC} is the unit construction cost of HVDC transmission per kilometer and N is the ratio of the installed capacity of the PHS facility to the reference transmission capacity, which was assumed to be identical to that used for HVAC transmission (6.38 GW). p_{DC} was set to 1.4 million USD per km (ref. 34). C_{conv} is the cost of one converter-station terminal, set to 2 million USD per GW (ref. 33). The factor of two accounts for converter stations located at both ends of the transmission link. HVDC transmission efficiency was calculated using:

$$\eta_{DC}(d) = 1 - \lambda_{DC} d - 2\eta_{conv} \quad (15)$$

where λ_{DC} is the distance-dependent HVDC line-loss coefficient and η_{conv} is the loss fraction of one converter terminal. λ_{DC} was set to 0.000035 km^{-1}, corresponding to 3.5%-line loss per 1000 km,[34] and η_{conv} was set to 0.008 per terminal.

Transmission-adjusted LCOS was evaluated across transmission distances ranging from 100 to 1200 km, consistent with the transmission radii used in the spatial storage time calculation. At each distance, the final transmission-adjusted LCOS was defined as the lower value obtained from the HVAC and HVDC options. For comparison, other storage technologies, including flywheels, lead-acid batteries, lithium-ion batteries, sodium-sulfur batteries, redox-flow batteries, hydrogen storage, and supercapacitors, can generally be deployed near or around urban load centers. Their economic value depends strongly on proximity to demand and grid access. Siting these storage technologies far from load centers would introduce unnecessary transmission costs and would usually reduce their competitiveness. We therefore calculated their transmission-adjusted LCOS using a representative 100 km transmission distance as a grid-connection benchmark and compared it with the distance-dependent transmission-adjusted LCOS of PHS.

4.8. Assumptions and applicability

Our methods build upon established hydrological and engineering frameworks, integrating high-resolution runoff routing, reservoir inundation simulations, and cost-based screening to provide a consistent global assessment of PHS. As with any global-scale analysis, the framework necessarily relies on a set of assumptions and screening parameters that define feasibility, standardize economic evaluation, and ensure internal consistency across regions and technologies.

We do not intend these assumptions to represent fixed engineering prescriptions or universally optimal design choices. We use them to define a conservative and internally consistent reference scenario for global assessment. Regional planning objectives, regulatory frameworks, environmental protection standards, and hydro-climatic conditions may justify tightening or relaxing individual constraints, which would affect the number, scale, and configuration of deployable PHS projects without altering the broader spatial patterns or system-level insights identified in this study. The framework identifies technically feasible PHS opportunities under explicit and quantifiable constraints but does not replace site-specific feasibility studies, stakeholder engagement, ecological assessment, or governance processes. Consequently, not all identified sites will, or should, be developed, and PHS deployment must remain aligned with local energy system needs and social priorities.

Author contributions

Conceptualization: R. X., Z. Z. Methodology: R. X. Investigation: R. X. Visualization: R. X. Funding acquisition: R. X., Z. Z., Y. C., D. Z. Project administration: R. X., Z. Z. Supervision: Z. Z., Y. C., D. Z. Writing – original draft: R.X. Writing – review and editing: R. X., Z. Z., A. D. Z., L. E. B., J. H., D. V. S., D. C., Y. C., T. D., Y. Z., P. L., Y. Y., M. P., D. Z.

Conflicts of interest

There are no conflicts of interest to declare.

Data availability

The geographic information and key attributes of the 104 971 candidate PHS projects identified in this study are available at https://doi.org/10.6084/m9.figshare.32288043.The discharge dataset is available at https://www.reachhydro.org/home/records/grades; the river network dataset is available at https://www.reachhydro.org/home/params/merit-basins; the DEM dataset is available at https://global-hydrodynamics.github.io/; the natural and mixed World Heritage Sites are available at https://www.arcgis.com/home/item.html?id=ef1ecce8fa3e41d89688be6199b5b32c; the WDPA database is available at https://www.protectedplanet.net/en; the tropical rainforest dataset is available at https://glad.umd.edu/dataset/primary-forest-humid-tropics; the population dataset is available at https://landscan.ornl.gov/; the peatland dataset is available at https://archive.researchdata.leeds.ac.uk/251/; the GDP dataset is available at https://datadryad.org/stash/dataset/doi:10.5061/dryad.dk1j0; the global soil dataset is available at https://www.fao.org/soils-portal/data-hub/soil-maps-and-databases/harmonized-world-soil-database-v12/en/; the Global Seismic Hazard Map is available at https://gmo.gfz-potsdam.de/, the global land cover data are available at https://www.esa-landcover-cci.org/?q= node/197; the ERA5-land dataset is available at https://cds.climate.copernicus.eu/datasets/reanalysis-era5-single-levels?tab=overview; and the global electricity dataset is available at https://figshare.com/articles/dataset/Global_1_km_1_km_gridded_revised_real_gross_domestic_product_and_electricity_consumption_during_1992-2019_based_on_calibrated_nighttime_light_data/17004523/1. All datasets are listed in the references and are also available from the corresponding author upon request.

Supplementary information is available. See DOI: https://doi.org/10.1039/d6ee01331g.

Code availability: the geographic information and key attributes of the 104 971 candidate PHS projects identified in this study are available at DOI: https://doi.org/10.6084/m9.figshare.32288043. All data are available in the main text or the supplementary materials. The data and code of this study are also available in a public repository at DOI: https://doi.org/10.6084/m9.figshare.32288085.

The scripts used to generate all results were written in MATLAB (R2025b).

Acknowledgements

This study was supported by the National Natural Science Foundation of China (grant no. 42401359 and 12572266), the Fundamental and Interdisciplinary Disciplines Breakthrough Plan of the Ministry of Education of China (No. JYB2025XDXM909), the International Cooperation and Exchange of the National Natural Science Foundation of China (grant no. 42361144001), the Shenzhen Science and Technology Project for Sustainable Development in Special Innovation (grant no. KCXFZ20230731093403008), the SUSTech High Level of Special Funds (grant no. G03034K001 and G030290001), and DC was supported by the Carbon Neutrality and Energy System Transformation (CNEST) Program of Tsinghua University (10008001). Additional support was provided by the Integrated Catchment Solutions Programme of the United Kingdom Natural Environment Research Council (grant no. NE/P011160/1, NERC), the Innovation Programme under the Marie Skłodowska-Curie grant agreement (grant no. 765553), and the Euro-FLOW project, funded by the Horizon 2020 research programme of the European Union. Alan Ziegler is supported *via* the Sustainable Pathways to Expand ASEAN Renewables project (Contract No. B48G660115), under the International Research Collaboration Program: P23 (S4) – Advancing Research Collaboration, Technology Development, and Innovation of Institutions/Research Centers with Strong International Networks; Sub-Project N48(S4P23): Developing International Collaboration Networks (Global Partnership). We acknowledge the High-Performance Computing Centers at Eastern Institute of Technology and the Center for Computational Science and Engineering at Southern University of Science and Technology for providing computing resources, and thank the Terrestrial Hydrology Research Group at Princeton University for providing the state-of-the-art global runoff dataset.

Notes and references

1 M. Meinshausen, J. Lewis, C. McGlade, J. Gütschow and Z. Nicholls, Realization of Paris Agreement pledges may limit warming just below 2 °C, *Nature*, 2022, **604**, 304–309.
2 H. L. van Soest, M. G. J. den Elzen and D. P. van Vuuren, Net-zero emission targets for major emitting countries consistent with the Paris Agreement, *Nat. Commun.*, 2021, **12**, 2140.
3 A. Lal and F. You, Advances and challenges in energy and climate alignment of AI infrastructure expansion, *Adv. Appl. Energy*, 2025, **20**, 100243.
4 J. Zhao, F. Li and Q. Zhang, Impacts of renewable energy resources on the weather vulnerability of power systems, *Nat. Energy*, 2024, **9**, 1407–1414.
5 L. Xu, K. Feng, N. Lin, A. T. D. Perera, H. V. Poor, L. Xie, C. Ji, X. A. Sun, Q. Guo and M. O'Malley, Resilience of renewable power systems under climate risks, *Nat. Rev. Electric. Eng.*, 2024, **1**, 53–66.
6 M. M. Hasan, R. Haque, M. I. Jahirul, M. G. Rasul, I. M. R. Fattah, N. M. S. Hassan and M. Mofijur, Advancing energy storage: The future trajectory of lithium-ion battery technologies, *J. Energy Storage*, 2025, **120**, 116511.
7 M. Shoaib, P. Vallayil, N. Jaiswal, P. I. V. Suba, S. Sankararaman, K. Ramanujam and V. Thangadurai, Advances in redox flow batteries - A comprehensive review on inorganic and organic electrolytes and engineering perspectives, *Adv. Energy Mater.*, 2024, **14**(32), 2400721.
8 R. Kunzig, How giant water batteries could make green power reliable, *Science*, 2024, **383**(6681), 359–363.
9 N. C. Papadakis, M. Fafalakis and D. Katsaprakakis, A review of pumped hydro storage systems, *Energies*, 2023, **16**(11), 4516.
10 W. Yang, Z. Zhao, J. I. Pérez-Díaz, J. D. Hunt, E. Vagnoni, J. K. Nøland, E. Quaranta, R. Wang, X. Li and Y. Cheng, Pumped storage hydropower operation for supporting clean energy systems, *Nat. Rev. Electric. Eng.*, 2025, **1**, 454–473.
11 International Hydropower Association, *2025 World Hydropower Outlook*, 2025.
12 E. Barbour, I. A. G. Wilson, J. Radcliffe, Y. Ding and Y. Li, A review of pumped hydro energy storage development in significant international electricity markets, *Renewable Sustainable Energy Rev.*, 2016, **158**, 112119.
13 International Energy Agency, *The battery industry has entered a new phase*, 2025.
14 M. Stocks, R. Stocks, B. Lu, C. Cheng and A. Blakers, Global atlas of closed-loop pumped hydro energy storage, *Joule*, 2021, **5**, 1.
15 S. Ali, R. A. Stewart, O. Sahin and A. S. Vieira, Integrated GIS-AHP-based approach for off-river pumped hydro energy storage site selection, *Appl. Energy*, 2023, **337**(1), 120914.
16 J. D. Hunt, E. Byers, Y. Wada, S. Parkinson, D. E. H. J. Gernaat, S. Langan, D. P. van Vuuren and K. Riahi, Global resource potential of seasonal pumped hydropower storage for energy and water storage, *Nat. Commun.*, 2020, **11**, 947.
17 P. Lin, M. Pan, H. E. Beck, Y. Yang, D. Yamazaki, R. Frasson, C. H. David, M. Durand, T. M. Pavelsky, G. H. Allen, C. J. Gleason and E. F. Wood, Global reconstruction of naturalized river flows at 2.94 million reaches, *Water Resour. Res.*, 2019, **55**, 6499–6516.
18 Y. Yang, D. Feng and H. E. Beck, *et al.*, Global daily discharge estimation based on grid long short-term memory (LSTM) model and river routing, *Water Resour. Res.*, 2025, **61**(6), e2024WR039764.
19 A. Khosravani, J. K. Sieving, B. W. Billings and K. M. Powell, Techno-economic analysis of long-duration energy storage integrated with high-penetration renewable energy systems, *Energy Rep.*, 2025, **14**, 4086–4110.
20 O. Schmidt, S. Melchior, A. Hawkes and I. Staffell, Projecting the future levelized cost of electricity storage technologies, *Joule*, 2019, **3**(1), 81–100.
21 O. Schmidt and I. Staffell, *Monetizing energy storage*, 2023.
22 R. Xu, Z. Zeng, M. Pan, A. D. Ziegler, J. Holden, D. V. Spracklen, L. E. Brown, X. He, D. Chen, B. Ye, H. Xu, S. Jerez, C. Zheng, J. Liu, P. Lin, Y. Yang, J. Zou, D. Wang,

M. Gu, Z. Yang, D. Li, J. Huang, V. Lakshmi and E. F. Wood, A global-scale framework for hydropower development incorporating strict environmental constraints, *Nature Water*, 2023, **1**, 113–122.

23 D. Farinotti, V. Round, M. Huss, L. Compagno and H. Zekollari, Large hydropower and water-storage potential in future glacier-free basins, *Nature*, 2019, **575**, 341–344.

24 D. E. H. J. Gernaat, P. W. Bogaart, D. P. van Vuuren, H. Biemans and R. Niessink, High-resolution assessment of global technical and economic hydropower potential, *Nat. Energy*, 2017, **2**, 821–828.

25 A. Ganter, T. H. Ruggles, P. Gabrielli, G. Sansavini and K. Caldeira, Utilizing curtailed wind and solar power to scale up electrolytic hydrogen production in Europe, *Environ. Sci. Technol.*, 2025, **59**, 3495–3507.

26 O. Savin, J. Baroth, C. Badina, S. Charbonnier and C. Bérenguer, Damage due to start-stop cycles of turbine runners under high-cycle fatigue, *Int. J. Fatigue*, 2021, **153**, 106458.

27 B. H. Xiao, K. Xiao, J. X. Li, C. F. Xiao, S. Cao and Z. Q. Liu, Flexible electrochemical energy storage devices and related applications: recent progress and challenges, *Chem. Sci.*, 2024, **15**, 11229–11266.

28 Enerdata. *Global & emission projection 2050*, https://eneroutlook.enerdata.net/total-electricity-generation-projections.html (accessed May 2026).

29 P. R. Brown and A. Botterud, The value of inter-regional coordination and transmission in decarbonizing the US electricity system, *Joule*, 2021, **5**, 1.

30 D. Tong, D. J. Farnham, L. Duan, Q. Zhang, N. S. Lewis, K. Caldeira and S. J. Davis, Geophysical constraints on the reliability of solar and wind power worldwide, *Nat. Commun.*, 2021, **12**, 6146.

31 U.S. Energy Information Administration, *Assessing HVDC Transmission for Impacts of Non-Dispatchable Generation*, 2018.

32 National Grid, *Electricity Transmission Cost Study*, 2012.

33 NextGen Highways, *Buried high-voltage direct current (HVDC) transmission is cost competitive*, 2022.

34 Australian Energy Market Operator, *AEMO 2021 Transmission Cost Report for Integrated System Plan*, Australia, 2021.

35 S. K. Suraparaju, M. Samykano, J. R. Vennapusa, R. K. Rajamony, D. Balasubramanian, Z. Said and A. K. Pandey, Challenges and prospectives of energy storage integration in renewable energy systems for net zero transition, *J. Energy Storage*, 2025, **125**, 116923.

36 S.-Y. Pan, S. W. Snyder, A. I. Packman, Y. J. Lin and P.-C. Chiang, Cooling water use in thermoelectric power generation and its associated challenges for addressing water-energy nexus, *Water-Energy Nexus*, 2018, **1**(1), 26–41.

37 V. Eyring, S. Bony, G. A. Meehl, C. A. Senior, B. Stevens, R. J. Stouffer and K. E. Taylor, Overview of the Coupled Model Intercomparison Project Phase 6 (CMIP6) experimental design and organization, *Geosci. Model Dev.*, 2016, **9**, 1937–1958.

38 B. Saulsbury, *A comparison of the environmental effects of open-loop and closed-loop pumped storage hydropower*, Pacific Northwest National Laboratory, 2020.

39 J. D. Hunt, C. V. Silva, E. Fonseca, M. A. V. de Freitas, R. Brandão and Y. Wada, Role of pumped hydro storage plants for flood control, *J. Energy Storage*, 2024, **104**, 114496.

40 B. Zakeri, J. D. Hunt, M. Laldjebaev, V. Krey, A. Vinca, S. Parkinson and K. Riahi, Role of energy storage in energy and water security in Central Asia, *J. Energy Storage*, 2022, **50**, 104587.

41 UNEP-WCMC, *User Manual for the World Database on Protected Areas and world database on other effective area-based conservation measures*, 2019.

42 IUCN and UNEP-WCMC, *UNESCO Natural and Mixed World Heritage Sites*, 2024.

43 S. Turubanova, P. V. Potapov, A. Tyukavina and M. C. Hansen, Ongoing primary forest loss in Brazil, Democratic Republic of the Congo, and Indonesia, *Environ. Res. Lett.*, 2018, **13**, 074028.

44 J. Xu, P. J. Morris, J. Liu and J. Holden, PEATMAP: Refining estimates of global peatland distribution based on a meta-analysis, *CATENA*, 2018, **160**, 134–140.

45 C. Lamarche, M. Santoro, S. Bontemps, R. D'Andrimont, J. Radoux, L. Giustarini, C. Brockmann, J. Wevers, P. Defourny and O. Arino, Compilation and validation of SAR and optical data products for a complete and global map of inland/ocean water tailored to the Climate Modeling Community, *Remote Sens.*, 2017, **9**(1), 36.

46 LandMark, *The global platform of Indigenous and Community Lands*, 2024, https://www.landmarkmap.org/.

47 United Nations, *United Nations Declaration on the Rights of Indigenous Peoples*, 2007.

48 F. B. Siqueira and M. A. dos Santos, Solutions proposed for socio-environmental conflicts and concerning multiple-use hydroelectric reservoirs in Brazil, *Environ. Prog. Sustainable Energy*, 2021, **40**(5), e13645.

49 I. G. Baird, R. A. M. Silvano, B. Parlee, M. Poesch, B. Maclean, A. Napoleon, M. Lepine and G. Hallwass, The downstream impacts of hydropower dams and indigenous and local knowledge: examples from the peace–Athabasca, Mekong, and Amazon, *Environ. Manage.*, 2021, **67**(1), 1–14.

50 J. Muñoz-Sabater, E. Dutra, A. Agustí-Panareda, C. Albergel, G. Arduini, G. Balsamo, S. Boussetta, M. Choulga, S. Harrigan, H. Hersbach, B. Martens, D. G. Miralles, M. Piles, N. J. Rodríguez-Fernández, E. Zsoter, C. Buontempo and J.-N. Thépaut, ERA5-Land: a state-of-the-art global reanalysis dataset for land applications, *Earth System Science Data*, 2021, **13**(9), 4349–4383.

51 D. Yamazaki, D. Ikeshima, R. Tawatari, T. Yamaguchi, F. O'Loughlin, J. C. Neal, C. C. Sampson, S. Kanae and P. D. Bates, A high-accuracy map of global terrain elevations, *Geophys. Res. Lett.*, 2017, **44**, 5844–5853.

52 D. Yamazaki, D. Ikeshima, J. Sosa, P. D. Bates, G. H. Allen and T. M. Pavelsky, MERIT Hydro: A high-resolution global hydrography map based on latest topography dataset, *Water Resour. Res.*, 2019, **55**, 5053–5073.

53 National Energy Administration, *Code for Design of Pumped Storage Power Stations (in Chinese)*, 2018.

54 U.S. Army Corps of Engineers, *Technical Analysis of Pumped Storage and Integration with Wind Power in the Pacific Northwest*, 2009.

55 Water Affairs and Forestry, *Republic of South Africa. Assessment of Pumped Storage and Hydropower Schemes*, 2009.
56 X. Lu and S. Wang, A GIS-based assessment of Tibet's potential for pumped hydropower energy storage, *Renewable Sustainable Energy Rev.*, 2017, **69**, 1045–1054.
57 N. Ghorbani, H. Makian and C. Breyer, A GIS-based method to identify potential sites for pumped hydro energy storage - Case of Iran, *Energy*, 2019, **169**, 854–867.
58 T. Soha, B. Munkácsy, Á. Harmat, C. Csontos, G. Horváth, L. Tamás, G. Csüllög, H. Daróczi, F. Sáfián and M. Szabó, GIS-based assessment of the opportunities for small-scale pumped hydro energy storage in middle-mountain areas focusing on artificial landscape features, *Energy*, 2017, **141**, 1363–1373.
59 A. Rogeau, R. Girard and G. Kariniotakis, A generic GIS-based method for small Pumped Hydro Energy Storage (PHES) potential evaluation at large scale, *Appl. Energy*, 2017, **197**, 241–253.
60 B. Lu, M. Stocks, A. Blakers and K. Anderson, Geographic information system algorithms to locate prospective sites for pumped hydro energy storage, *Appl. Energy*, 2019, **222**, 300–312.
61 H. Zhao, Y. Xin, S. Liu, X. Li, M. Wang, G. Ou, T. Wang, Q. Yang, Q. Shi and F. Liu, Method for calculating frozen storage capacity of reservoir of pumped storage power station in cold and severe cold areas, China Patent CN107067339B, 2017.
62 V. Lebakula, K. Sims, A. Reith, A. Rose, J. McKee, P. Coleman, J. Kaufman, M. Urban, C. Jochem, C. Whitlock, M. Ogden, J. Pyle, D. Roddy, J. Epting and E. Bright, LandScan Global 30 Arcsecond Annual Global Gridded Population Datasets from 2000 to 2022, *Sci. Data*, 2025, **12**, 495.
63 G. Fischer, F. O. Nachtergaele, S. Prieler, E. Teixeira, G. Tóth, H. van Velthuizen, L. Verelst and D. Wiberg, *Global agro-ecological zones assessment for agriculture (GAEZ 2008)*, IIASA, Laxenburg, Austria and FAO, 2008.
64 K. M. Shedlock, D. Giardini, G. Grunthal and P. Zhang, The GSHAP Global Seismic Hazard Map, *Seismol. Res. Lett.*, 2000, **71**(6), 679–686.
65 United States Department of Agriculture, *Land Values 2024 Summary*, 2024.
66 Farm Credit Canada, *2023 FCC Farmland Values Report*, 2024.
67 Eurostat, *Agricultural land prices and rents – statistics*, 2024.
68 M. Kummu, M. Taka and J. H. A. Guillaume, Gridded global datasets for Gross Domestic Product and Human Development Index over 1990–2015, *Sci. Data*, 2018, **5**, 180004.
69 J. Li, S. Zhang, C. Wang, Z. Jiang, J. Zheng, X. Wang and T. Lu, Investigation on large-scale 3D seepage characteristics of a pumped-storage power station: a case study in Zhejiang Province, China, *Water Sci. Technol.*, 2023, **88**(6), 1374–1393.
70 K. Miao, Z. Bai, Y. Huang, Y. Huang and Y. Su, Research on seepage control of Jurong pumped storage hydroelectric power station, *Water*, 2022, **14**(2), 141.
71 N. L. Poff and J. H. Matthews, Environmental flows in the Anthropocence: past progress and future prospects, *Curr. Opin. Environ. Sustainability*, 2013, **5**(6), 667–675.
72 A. V. Pastor, F. Ludwig, H. Biemans, H. Hoff and P. Kabat, Accounting for environmental flow requirements in global water assessments, *Hydrol. Earth Syst. Sci.*, 2014, **18**, 5041–5059.
73 M. Acreman, Environmental flows-basics for novices, *Wiley Interdiscip. Rev.: Water*, 2016, **3**(5), 622–628.
74 J. Chen, M. Gao, S. Cheng, W. Hou, M. Song, X. Liu and Y. Liu, Global 1 km × 1 km gridded revised real gross domestic product and electricity consumption during 1992–2019 based on calibrated nighttime light data, *Sci. Data*, 2022, **9**, 202.